

Active Matrix Flexible Sensory Systems: Materials, Design, Fabrication, and Integration

Bin Bao, Dmitriy D. Karnaushenko, Oliver G. Schmidt,* Yanlin Song,*
and Daniil Karnaushenko*

A variety of modern applications including soft robotics, prosthetics, and health monitoring devices that cover electronic skins (e-skins), wearables as well as implants have been developed within the last two decades to bridge the gap between artificial and biological systems. During this development, high-density integration of various sensing modalities into flexible electronic devices becomes vitally important to improve the perception and interaction of the human bodies and robotic appliances with external environment. As a key component in flexible electronics, the flexible thin-film transistors (TFTs) have seen significant advances, allowing for building flexible active matrices. The flexible active matrices have been integrated with distributed arrays of sensing elements, enabling the detection of signals over a large area. The integration of sensors within pixels of flexible active matrices has brought the application scenarios to a higher level of sophistication with many advanced functionalities. Herein, recent progress in the active matrix flexible sensory systems is reviewed. The materials used to construct the semiconductor channels, the dielectric layers, and the flexible substrates for the active matrices are summarized. The pixel designs and fabrication strategies for the active matrix flexible sensory systems are briefly discussed. The applications of the flexible sensory systems are exemplified by reviewing pressure sensors, temperature sensors, photodetectors, magnetic sensors, and biosignal sensors. At the end, the recent development is summarized and the vision on the further advances of flexible active matrix sensory systems is provided.

1. Introduction

In recent years, flexible sensors have become one of the key research topics among the flexible electronics.^[1–3] Flexible sensors are lightweight, bendable, and conformable to uneven surfaces such as the human bodies and the robotic surfaces, opening a new path for the next generation of artificial electronic skins (e-skins). E-skins integrated with various sensor networks have provided a soft platform for the development of human machine interfaces, robotics, and prosthetics.^[4–6] Human-friendly wearable and implantable sensors can be seamlessly integrated into the body to monitor vital sign signals, enabling a better healthcare management for the patients with chronic diseases. As one of the enabling technologies for the “Internet of Things (IoT),” the flexible sensors can be distributed on the target surfaces to detect external stimuli and remotely provide information through the network of interconnections. Among these flexible sensors, devices with single sensing elements have been intensively studied. However, to collect signals over a large area, sensor arrays with many distributed

B. Bao, D. D. Karnaushenko, D. Karnaushenko
Institute for Integrative Nanosciences
Leibniz IFW Dresden
01069 Dresden, Germany
E-mail: d.karnaushenko@ifw-dresden.de

O. G. Schmidt
Center for Materials
Architectures and Integration of Nanomembranes (MAIN)
Chemnitz University of Technology
09126 Chemnitz, Germany
E-mail: oliver.schmidt@main.tu-chemnitz.de

 The ORCID identification number(s) for the author(s) of this article can be found under <https://doi.org/10.1002/aisy.202100253>.

© 2022 The Authors. Advanced Intelligent Systems published by Wiley-VCH GmbH. This is an open access article under the terms of the Creative Commons Attribution License, which permits use, distribution and reproduction in any medium, provided the original work is properly cited.

DOI: 10.1002/aisy.202100253

O. G. Schmidt
Material Systems for Nanoelectronics
Chemnitz University of Technology
09107 Chemnitz, Germany

O. G. Schmidt
Nanophysics
Faculty of Physics
TU Dresden
01062 Dresden, Germany

Y. Song
Beijing National Laboratory for Molecular Sciences (BNLMS)
Key Laboratory of Green Printing
Institute of Chemistry
Chinese Academy of Sciences
Beijing 100190, P. R. China
E-mail: ylsong@iccas.ac.cn

pixels are desired. The sensor arrays add new dimensions to the measurement, enabling spatiotemporal mapping of the detected signals.^[7] Large quantities of data collected by the sensor arrays could be analyzed with the help of artificial intelligence (AI), allowing to gather valuable information for the feedback control of robotics as well as the health monitoring and diagnostics of patients.^[8]

By increasing the number of pixels, direct addressing of individual sensors within the flexible systems becomes much more difficult due to the dramatic increase in the number of interconnects. This, as a consequence, influences the mechanical flexibility of the system. Therefore, a proper addressing approach is crucial for the integration of large-area flexible sensor arrays with high pixel density. So far, two addressing technologies, namely, the passive matrix addressing and the active matrix addressing, are widely used for displays which have also been explored for sensory systems.^[9,10] The passive way of addressing is simple from the design and fabrication points of view, but suffers from large crosstalk, slow rate, and high power consumption.^[11] In contrast, the active way of addressing relies on integrated switching elements such as thin-film transistors (TFTs) within each pixel of the active matrix, which effectively lowers signal crosstalk, improves response time, and reduces power consumption.^[12] With the active matrix addressing approach, the individual pixels within the flexible sensory system can be selected exclusively for signal readout while the others are deactivated. Moreover, the active matrix backplane provides an ideal platform for the heterogeneous integration of different sensing elements with high pixel density, equipping the flexible electronics such as the e-skins with multifunctional sensing

modalities which could have augmented capabilities compared to their nature counterparts (Figure 1).

Flexible TFT technologies lie at the heart of flexible electronics.^[13] During the last two decades, the fast development of flexible TFT technologies has enabled the realization of various active matrix flexible sensors.^[14,15] TFTs based on different material combinations have been integrated to address the pixels in the flexible sensory systems, bringing the flexible sensors to a high level of sophistication with many advanced functionalities. Meanwhile, it puts extremely high demands in the performance of the component TFTs when they are integrated into the active matrix flexible sensory systems. For example, to decrease the signal crosstalk between adjacent pixels, the on/off ratio of the TFTs should be as high as possible, which means the TFTs should keep a high on current while keeping an extremely low off current. The large on/off ratio can also lower the power consumption of the sensors. For a fast readout of the detection signals, the mobility of the TFTs should be high enough. To achieve a stable operation of the active matrix sensory system, the variations of the electrical performance for the TFTs should be small. Among these variations, the shift of the threshold voltage (V_{th}) is one of the main focuses. For a specific application of the active matrix sensory systems, the electrical performance of the component TFTs should be orthogonal to the influence of the detecting physical parameters. For example, the TFTs in the active matrix temperature sensors should be stable within the operating temperature range. Figure 2 summarizes a brief timeline to show some key examples of the active matrix flexible systems. Since the first report on large-area plastic active matrix backplane circuit in 2001,^[16] the active matrix sensors have

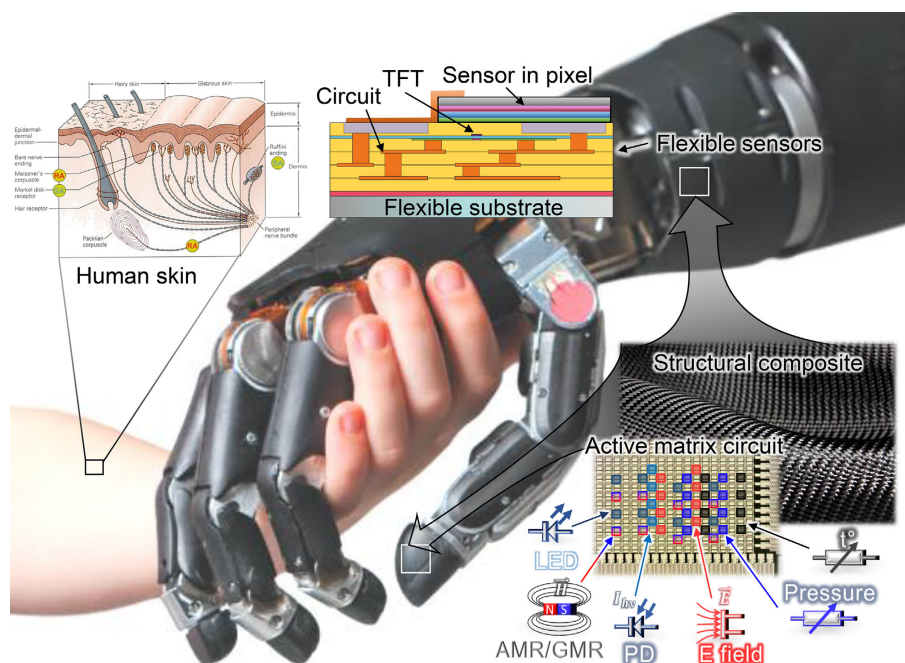


Figure 1. Heterogeneous integration of flexible sensors on the active matrix platform for the e-skin applications. Various sensors can be heterogeneously integrated with the active matrix driving circuit to create a flexible sensory system, equipping the e-skins with multifunctional sensing modalities. Reproduced with permission.^[184] Copyright 2013, Macmillan Publishers Ltd., Reproduced with permission.^[185] Copyright 2000, McGraw-Hill Companies.

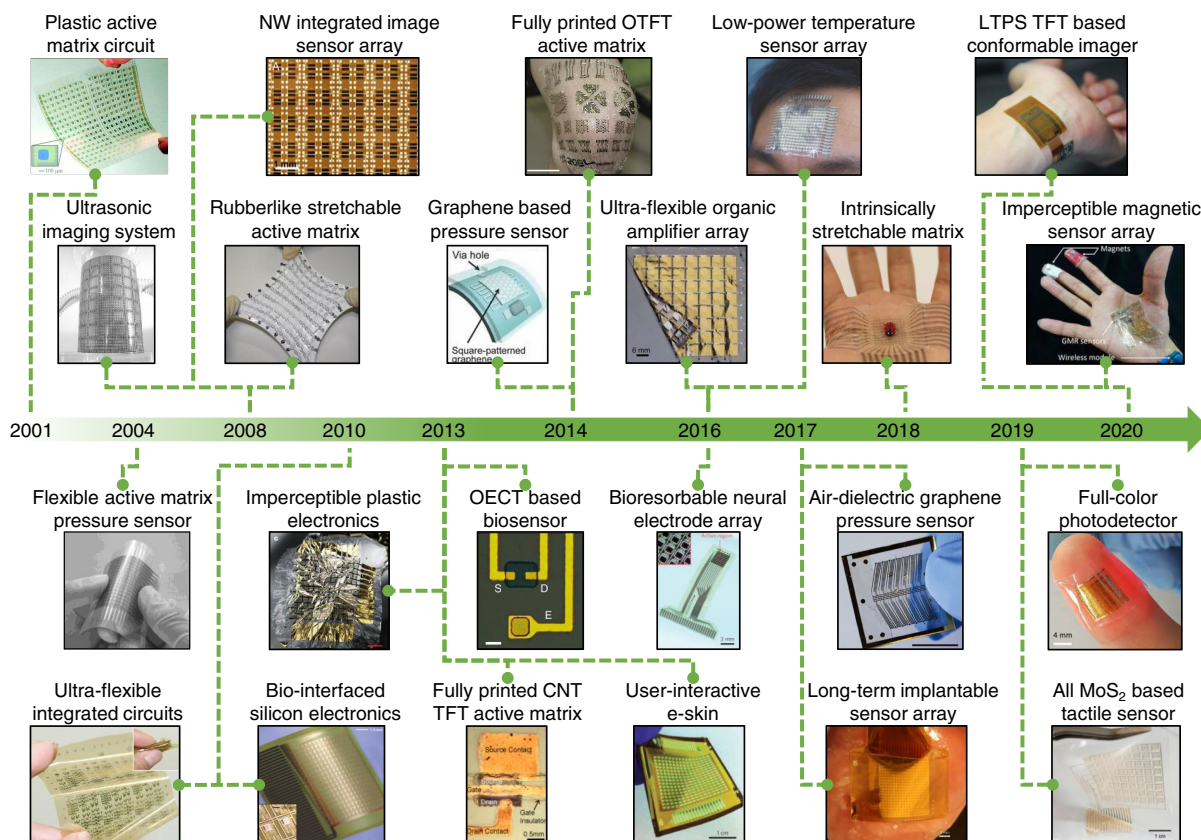


Figure 2. A brief timeline showing some key examples of the active matrix flexible sensory systems. Adapted with permission: “Plastic active matrix circuit.”^[16] Copyright 2001, National Academy of Sciences. “Flexible active matrix pressure sensor.”^[64] Copyright 2004, National Academy of Sciences. “Ultrasonic imaging system.”^[186] Copyright 2008, IEEE. “NW integrated image sensor array.”^[94] Copyright 2008, National Academy of Sciences. “Rubberlike stretchable active matrix.”^[19] Copyright 2008, American Association for the Advancement of Science. “Ultraflexible integrated circuits.”^[17] Copyright 2010, Macmillan Publishers Ltd. “Bio-interfaced silicon electronics.”^[41] Copyright 2010, American Association for the Advancement of Science. “Imperceptible plastic electronics.”^[18] Copyright 2013, Macmillan Publishers Ltd. “OECT based biosensor.”^[20] Copyright 2013, Macmillan Publishers Ltd. “Fully printed SWCNT TFT active matrix.”^[30] Copyright 2013, American Chemical Society. “User-interactive e-skin.”^[89] Copyright 2013, Macmillan Publishers Ltd. “Graphene based pressure sensor.”^[97] Copyright 2014, Wiley-VCH Verlag GmbH & Co. KGaA. “Fully printed OTFT active matrix.”^[31] Copyright 2014, Macmillan Publishers Ltd. “Ultra-flexible organic amplifier array.” Reproduced under the terms of the CC BY license.^[71] Copyright 2017, The Authors. Springer Nature. “Bioresorbable neural electrode array.”^[42] Copyright 2016, Macmillan Publishers Ltd. “Low-power temperature sensor array.”^[12] Copyright 2016, Wiley-VCH Verlag GmbH & Co. KGaA. “Air-dielectric graphene pressure sensor.”^[98] Reproduced under the terms of the CC BY license.^[98] Copyright 2017, The Authors. Springer Nature. “Long-term implantable sensor array.”^[26] Copyright 2017, Macmillan Publishers Ltd. “Intrinsicly stretchable matrix.”^[80] Copyright 2018, Macmillan Publishers Ltd., part of Springer Nature. “Full-color photodetector.”^[129] Reproduced with permission.^[129] Copyright 2019, Science Advances. “All MoS₂ based tactile sensor.”^[100] Copyright 2019, American Chemical Society. “LTPS TFT based conformable imager.”^[24] Copyright 2020, Springer Nature Ltd. “Imperceptible magnetic sensor array.”^[27] Copyright 2020, The Authors. Published by AAAS.

become ultraflexible,^[17] imperceptible,^[18] stretchable,^[19] implantable,^[20] and large-area printable^[21] with low power consumption and functionalities ranging from pressure sensing, temperature mapping, and photodetection, to magnetic field mapping and biosignal monitoring.

In **Figure 3**, we present a vision on how the active matrix flexible sensory systems should be organized. In these systems, the active matrix backplanes are essential components to reliably drive individual sensors and readout the signals. The backplanes consist of several key building blocks, where each of the blocks was optimized to realize integrated active matrices with excellent electrical and mechanical performance. We envision that such active matrix sensory systems should integrate heterogeneous

sensing elements such as piezoresistors,^[18] thermistors,^[22] magnetoresistors,^[23] photodiodes,^[24] light-emitting diodes (LEDs),^[25] and electrical field sensors^[26] within individual pixels, providing multifunctional sensing modalities. So far, most of the reported active matrix flexible sensory systems can only perceive one kind of stimulus. For example, pressure sensors, temperature sensors, photodetectors, magnetic sensors, and biosignal sensors have been reported by incorporating the corresponding sensing elements into the active matrices. To generate multiperceptual sensory systems, more than one of these sensing modalities should be heterogeneously integrated into the same active matrices in the future. The flexible sensory systems are interfaced to the external circuits through flexible flat cable (FFC) connections

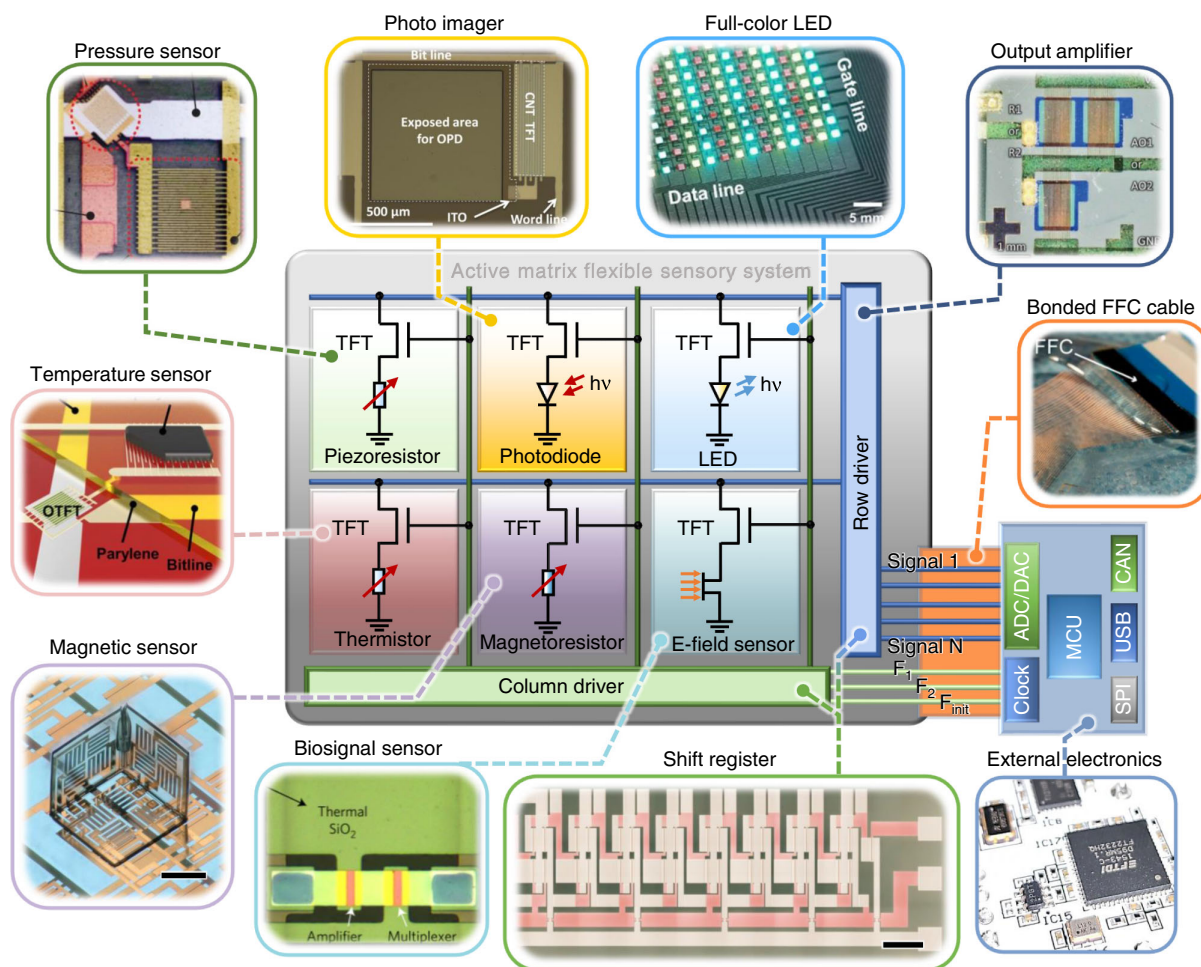


Figure 3. Vision of the active matrix flexible sensory systems. Different sensing elements such as piezoresistors, thermistors, magnetoresistors, photodiodes, LEDs, and electrical field sensors can be heterogeneously integrated into the pixels of the active matrix, creating a sensory system with multi-functional sensing modalities. Typical active matrix flexible sensors include pressure sensors, temperature sensors, photodetectors, magnetic sensors, and biosignal sensors. The flexible sensory systems are interfaced to the external circuits through FFC connections. Column and row drivers such as shift registers and output amplifiers can also be on-chip integrated to decrease the number of interconnects. Adapted with permission: “Pressure sensor.”^[18] Copyright 2013, Macmillan Publishers Ltd. “Temperature sensor.”^[22] Copyright 2015, The Authors. Published under the PNAS license. “Magnetic sensor.”^[23] Copyright, The Authors. Published by Springer Nature. “Biosignal sensor.”^[26] Copyright 2017, Macmillan Publishers Ltd., part of Springer Nature. “Bonded FFC cable.”^[187] Copyright 2020, The Authors. Published by National Academy of Sciences. “Output amplifier.”^[27] Copyright 2020, The Authors. Published by AAAS. “Full-color LED.”^[25] Reproduced with permission.^[25] Copyright 2020, AAAS. “Photo imager.”^[24] Copyright 2020, Springer Nature Ltd. “Shift register,” “External electronics”: images courtesy of Daniil Karnausenko.

for power supply, clocking as well as data acquisition and processing. To further improve the flexibility of the sensory systems, column and row drivers such as shift registers and output amplifiers could be integrated onto the flexible platform.^[27] By integrating the decoders and shift registers, the number of the final interconnects with the external circuits can be effectively reduced which can further enhance the mechanical flexibility of the system and improve the design freedom in the final applications.

To realize the active matrix flexible sensory systems, various functional materials have been integrated by different fabrication strategies such as conventional photolithography,^[28] shadow mask-assisted deposition,^[29] and large-area printing technologies.^[30–33] Meanwhile, specific material integration

and device fabrication strategies have to be adopted depending on the material properties and the application requirements. Herein, we present a review of the recent progress in the area of active matrix flexible sensory systems with a focus on materials, designs, fabrication strategies, and applications. We will first discuss materials used for the flexible active matrix backplanes, with an emphasis on the semiconductor channel materials, dielectric materials, and flexible substrates. Then, we briefly discuss the pixel circuit designs. The fabrication strategies for the active matrix flexible sensory systems are also described. Finally, the applications of the sensory systems will be reviewed by taking pressure sensors, temperature sensors, photodetectors, magnetic sensors, and biosignal sensors as examples. At the end

of the review, we summarize the recent development and provide an outlook on how the active matrix flexible sensory systems can be advanced further.

2. Materials for the Active Matrix Flexible Sensory Systems

Different from their rigid counterparts, the active matrix flexible sensory systems are constructed by a combination of materials which are soft, flexible, bendable, and even stretchable. Normally the flexible sensors are fabricated beginning with a rigid handling substrate, onto which the flexible substrate is attached. After the fabrication, the devices are released and rendered the form factor of flexibility.^[34–36] Typical materials to construct the TFT elements include the gate, source, and drain conducting contacts, the gate dielectric materials and the semiconductor channel materials.^[37] The most frequently used conductor materials for the active matrix backplanes are still metal thin films, although there are already a lot of reports on other flexible conductors such as graphene, metal oxides, silver nanowires, and carbon nanotubes (CNTs).^[38] The sensing element materials are diverse, depending on the specific sensing functions as required. Therefore, in this section we focus on the semiconductor channel materials, gate dielectrics, and flexible substrate materials for the active matrix backplanes.

2.1. Semiconductor Channel Materials

Semiconductor channel materials play a crucial role in determining the electrical performance of the active matrices, such as the mobility and the on/off ratio which are the most important parameters for the TFT operation.^[39,40] With high mobility the TFTs can be operated with high frequency, enabling high-speed signal readout for the sensors. Larger on/off ratio will lead to less possibility of signal crosstalk and lower power consumption. Therefore, TFTs with large mobility and high on/off ratio are ideal components for the active matrix backplanes. However, for real applications other factors such as the material compatibility, available fabrication facilities and prices have also to be considered. As a result, various semiconductors have been reported as the channel materials for the active matrix backplanes in flexible sensors, as listed in Table 1.

2.1.1. Silicon-Based Semiconductors

Silicon-based semiconductors, including monocrystalline,^[26,41–47] low-temperature polycrystalline,^[24,48] and amorphous^[49–54] silicon, have been used as the channel materials in the active matrix flexible sensory systems. The monocrystalline silicon (m-Si) has a mobility as high as $1000 \text{ cm}^2 \text{ V}^{-1} \text{ s}^{-1}$.^[55] However, the rigid form factor prohibits its applications in flexible electronics. To overcome this limitation, transfer printing of m-Si nano-membranes has been proposed.^[56] The doped m-Si ribbons are first fabricated on silicon wafer and then transfer-printed to plastic substrates. The high quality of the m-Si ensures the fast operation of the obtained TFT active matrices.^[43] Although m-Si shows great potential in high-end flexible sensors, the expensive doping and

fabrication processes limit its broad applications in consumer electronics. Recently, low-temperature polycrystalline silicon (p-Si) and amorphous silicon (a-Si:H) have also been reported as channel materials for driving flexible sensors such as conformable imagers and pressure sensors.^[24,52] The application of a-Si:H in flexible sensors would decrease the production price at a cost of relatively low mobility. a-Si:H TFTs have a typical mobility of $\approx 1 \text{ cm}^2 \text{ V}^{-1} \text{ s}^{-1}$, which is sufficient for the driving of normal consumer electronics.^[57]

2.1.2. Organic Semiconductors

Organic thin-film transistors (OTFTs) are considered as promising components for the next-generation electronic devices,^[58–61] and organic semiconductors have been extensively reported as channel materials to construct organic active matrices for flexible sensors.^[62] The organic semiconductors can be deposited at low temperature which is compatible to plastic substrates. Their solution processable property enables low-cost large-area fabrication.^[63] Their intrinsic flexibility offers the possibility to realize ultraflexible and foldable active matrix backplanes, which are essential for the imperceptible sensors.^[18] So far, two small molecular organic semiconductors, namely, pentacene^[64,65] and dinaphtho[2,3-b:2',3'-f]thieno[3,2-b]thiophene (DNNT),^[18,22,66] are mostly explored as the channel materials for OTFT active matrix flexible sensors. The reported organic active matrix flexible sensors include pressure sensors,^[64–68] image scanners,^[69,70] temperature sensors,^[12,22] magnetic sensors^[27] and biosignal sensors,^[20,71–74] to name a few. One disadvantage of the organic semiconductors is that they are sensitive to air, moisture, and common solvents used during photolithographic process.^[75] Therefore, special fabrication strategies that are compatible with these materials should be considered, and proper encapsulation needs to be adopted to increase their long-term stability.^[76]

Conjugated polymers such as polypyrrole (PPy), polythiophene (PTh), and polyaniline (PAN) have been widely used in electronic devices due to their intrinsic electron conductivity.^[77] Meanwhile, these materials can change their conductivity significantly through ionic doping. Therefore, they can be used as channel materials to construct organic electrochemical transistors (OECTs).^[78] Conducting polymer poly(3,4-ethylenedioxythiophene)-polystyrene sulfonate (PEDOT:PSS) has been used as channel material in OECTs and the obtained PEDOT:PSS OECT active matrix multielectrode arrays are used to spatially map the weak electrophysiological signals in vivo with substantial amplification.^[79]

The organic semiconductors can be designed with intrinsically stretchable property due to their versatility in molecular modification. OTFT active matrix flexible sensors with intrinsically stretchable semiconductor channels have been demonstrated by a few groups.^[80–82] Although the intrinsically stretchable TFTs are still in their infancy, and standard protocols for material synthesis and device fabrication need to be developed, sensor devices based on intrinsically stretchable semiconductors have already demonstrated superiority in integration density and mechanical robustness over their geometric design counterparts with rigid materials.^[83]

Table 1. Typical semiconductor materials for active matrix flexible sensory systems.

Semiconductor type	Channel material	Mobility ($\text{cm}^2\text{V}^{-1}\text{s}^{-1}$)	On/off ratio	Patterning method	Sensor type	Reference
Silicon-based materials	m-Si	≈ 490	$\approx 10^5$	Transfer printing and photolithography	Biosignal sensors	[26,41-44]
		≈ 350	$> 10^3$			
		≈ 400	$\approx 10^8$			
		≈ 800	$\approx 10^7$			
		≈ 600	$\approx 10^7$			
	m-Si	661	$> 10^6$	Transfer printing and photolithography	Tactile sensor	[45]
m-Si	≈ 470	4×10^5	Transfer printing and photolithography	Pressure sensor	[46]	
p-Si	40	10^7	Photolithography	Conformable imager	[24]	
a-Si:H	–	–	Deposition with inkjet-printed masks	Imager array	[49,50]	
a-Si:H	≈ 0.5	$> 10^7$	Photolithography	Pressure and temperature sensor	[51,52]	
Organic materials	Pentacene	1–1.4	10^5 – 10^6	Shadow mask	Pressure sensors	[29,64]
	Pentacene	0.7	10^4 – 10^5	Shadow mask	Image scanner	[69]
	Pentacene	0.7	$> 10^6$	Inkjet printing	Pressure sensor	[67]
	Pentacene	≈ 0.5	10^7	Inkjet printing	Ultrasonic sensor	[188]
	Pentacene	0.5	$> 10^4$	Shadow mask	Pressure sensor	[17]
	Pentacene	0.2	$> 10^6$	Photolithography	X-Ray imager	[115]
	DNTT	1.7	$> 10^7$	Shadow mask	Pressure sensor	[18,66,135]
	DNTT	2.2	$> 10^8$	Shadow mask	Temperature sensor	[22]
	DNTT	0.24	10^6	Shadow mask	Biosignal sensors	[71,72]
	DNTT	0.5	10^4 – 10^5	Shadow mask and screen printing	Temperature sensor	[12]
	DNTT	0.7 ± 0.2	5×10^3	Shadow mask and screen printing	Pyroelectric sensor	[162]
	DNTT	0.253 ± 0.012	$\approx 10^7$	Shadow mask	Magnetic sensor	[27]
	PEDOT:PSS	–	–	Screen and inkjet printing	Temperature and pressure sensor	[189]
	Inorganic oxides	PEDOT:PSS	–	–	Photolithography	Biosignal sensors
P3HT nanofibrils		7.45	4.1×10^4	Spin coating through shadow mask	Tactile sensor	[81]
IGZO		10–15	$\approx 10^7$	Photolithography	X-Ray detector	[124,170]
Nanotubes and nanowires	IGZO	≈ 12	–	Photolithography and printing	Photodetector	[160]
	IGZO	10.75–22.01	–	Photolithography	Photodetector	[190]
	IGZO	20	10^7	Photolithography	Piezoelectric sensor	[191]
	IGZO	14.4 ± 4.6	$> 10^6$	Photolithography	Optical image sensor	[111]
	IGZO	12.51 ± 1.32	1.1×10^8	Photolithography	Magnetic sensor	[23]
	SWCNT	18–27	$\approx 10^4$	Photolithography	Pressure sensor	[89,112]
2D materials	SWCNT	≈ 20	$\approx 10^5$	Photolithography	X-Ray imager	[91]
	SWCNT	0.8 ± 0.3	$\approx 10^4$	Gravure printing	Tactile sensor	[21]
	SWCNT	0.015–0.027	$\approx 10^3$	Roll-to-roll printing	Tactile sensor	[32]
	SWCNT	17.6	$> 10^5$	Photolithography	Pressure sensor	[90]
	Ge/Si NW	30–120	–	Transfer printing and photolithography	Imager sensor	[94]
	Ge/Si NW	≈ 20	–	Transfer printing and photolithograph	Pressure sensor	[95]
	Graphene	477 (p-type), 166 (n-type)	–	Photolithography	Pressure sensor	[97]
	Graphene	498 (p-type), 178 (n-type)	10	Photolithography	Strain sensor	[99]
	Graphene	212 (p-type), 96 (n-type)	–	Photolithography	Pressure sensor	[98]
	MoS ₂	≈ 40	$\approx 10^6$	Photolithography	Humidity sensor	[101]
	MoS ₂	$\approx 16.2 \pm 1.3$	$\approx 10^6$	Photolithography	Tactile sensor	[100]

2.1.3. Inorganic Oxide Semiconductors

Since the first report on the amorphous indium-gallium-zinc oxide (a-IGZO) TFTs with considerable mobility in 2004, significant attention has been paid to amorphous oxide TFTs.^[35,84,85] The amorphous oxide semiconductors exhibit mobilities similar to their crystalline counterparts due to the large overlapping of the isotropically spread metal *s*-orbitals.^[84] a-IGZO is a competitive candidate as the channel material for active matrix flexible sensors owing to its high mobility, good uniformity, and low processing temperature.^[37] Moreover, a-IGZO is compatible with the conventional photolithographic process which enables an easy sensor manufacturing workflow.^[86] It needs to point out that the a-IGZO TFTs are sensitive to oxygen and moisture during operation; therefore, a proper passivation layer is necessary to increase the device stability.^[87] Although a-IGZO is the only reported oxide semiconductor for the active matrix flexible sensors so far, other inorganic oxides including some binary and ternary metal oxide semiconductors would also have potential in sensor applications. Moreover, the recently reported solution processable fabrication routes of these oxide TFTs will eliminate the necessity of expensive vacuum facilities, thus enabling large-area fabrication of flexible sensor arrays with low price.^[85]

2.1.4. Nanotubes and Nanowires

Semiconductor-enriched single-walled carbon nanotubes (SWCNTs) have been extensively reported as a high-performance channel material for TFTs due to their high carrier mobility, low operation voltage, and solution processability.^[88] Moreover, the small diameters of the nanotubes make their randomly distributed networks mechanically flexible and stretchable. Large-area fully printed flexible SWCNT TFT active matrix backplanes have been reported.^[30,32] The obtained backplanes are used for driving pressure sensors^[21,89,90] and X-Ray imagers.^[91] One of the key challenges for the scalable fabrication of high-performance SWCNT TFT active matrices for flexible sensors is the sorting of the SWCNTs. Batch-produced CNTs contain a mixture of semiconducting and metallic SWCNTs. Therefore, sorting of the SWCNTs is critical to decrease the off current of the SWCNT TFTs.^[92] Density gradient ultracentrifugation technique has been used to produce highly semiconductor-enriched (99%) SWCNTs.^[93] For large-area fabrication of high-performance devices, more efficient sorting techniques to achieve higher degree of purity are desired in the future.

In addition to CNTs, other 1D nanomaterials such as Ge/Si core/shell nanowires have been used to construct nanowire TFT active matrices for pressure and image sensors.^[94,95] The Ge/Si nanowire TFTs exhibit a field-effect mobility of $20 \text{ cm}^2 \text{ V}^{-1} \text{ s}^{-1}$ with a low operation voltage of less than 5 V. Due to the inherent flexibility of the nanowires, the obtained sensors show excellent mechanical robustness and reliability.

2.1.5. 2D Materials

2D materials, which consist of just a single layer of atoms, are finding a growing number of applications in flexible and conformal electronics because of their unique properties such as

exceptional electronic performance, large surface to volume ratio, and high mechanical compliance.^[96] So far, graphene^[97–99] and monolayer molybdenum disulfide (MoS_2)^[100,101] are two kinds of reported 2D materials used for active matrix flexible sensory systems. Although graphene has excellent electron and hole mobilities, the graphene TFTs cannot be totally switched off due to the lack of a bandgap, and the on/off ratios of graphene TFTs are generally small.^[102] Therefore, graphene TFTs are more often integrated in the flexible sensors with specially designed device architectures. Monolayer MoS_2 is a direct bandgap semiconductor with large electron mobility.^[103] Since the first report on monolayer MoS_2 TFT with a mobility of at least $200 \text{ cm}^2 \text{ V}^{-1} \text{ s}^{-1}$, MoS_2 TFT active matrix backplanes have been rising as a promising driving technology for flexible displays and sensors.^[25,100,101,104] For example, all MoS_2 -based large-area, skin attachable active matrix tactile sensor has been reported, where the MoS_2 functions as a semiconductor channel and a resistive pressure gauge.^[100] Highly sensitive MoS_2 humidity sensor array has been fabricated by taking advantage of its high response to the surface-adsorbed water molecules.^[101] So far, chemical vapor deposition (CVD) dominates the fabrication methods for wafer-scale high-quality MoS_2 . The wide application of MoS_2 TFT active matrices in flexible sensors is highly dependent on the CVD growth of uniform monolayer MoS_2 in large area with affordable price. Besides, the 2D materials are normally grown on specific substrates.^[105] Transferring the 2D materials to target flexible substrates with good quality and high yield is crucial to realize the 2D material-based electronic devices.^[106]

2.2. Gate Dielectric Materials

Flexible gate dielectric materials with excellent insulating and capacitive properties are another critical component for flexible TFTs. Various gate dielectric materials including inorganic, organic, organic/inorganic hybrid, ionic, and air-based dielectrics have been explored in the active matrix flexible sensory systems, as listed in **Table 2**. Several requirements for the gate dielectrics should be fulfilled to achieve high-performance active matrix backplanes for the flexible sensors. First, the power consumption, which is highly dependent on the dielectric layers, should be as low as possible because the flexible and wearable electronics are normally powered by portable batteries whose lifetime is still one of the obstacles limiting the long-term operation of these devices.^[12] To address this problem, high- κ ($\kappa > 3.9$) dielectrics have been developed.^[107] The implementation of high- κ dielectrics allows to further miniaturize the TFT size and decrease the operation voltage while keeping the leakage current low. Second, the dielectric materials should be electronically clean and possess a good interface with the semiconductor channel materials. The defect-free dielectric layer will eliminate the hysteresis behaviors of the TFTs while the clean interface will promote fast charge transport.^[108,109] Third, the gate dielectric materials should withstand substantial mechanical strain when the sensors are bent or folded. Currently, the dielectric failure is one of the most frequently reported failure modes for flexible TFTs.^[37] Therefore, special attention should be paid to their mechanical compliance when

Table 2. Typical gate dielectric materials for active matrix flexible sensory systems.

Dielectric type	Dielectric material	Thickness [nm]	Operation voltage [V]	Deposition method	Sensor type	Reference	
Inorganic dielectrics	SiO ₂	100	5	PECVD	Biosignal sensor	[41-43]	
	SiO ₂	160	5	PECVD	X-Ray detector	[170]	
	SiO ₂	70	10	PECVD	Conformable imager	[24]	
	SiN _x	290	15	PECVD	Pressure and temperature sensor	[52]	
	SiN _x	200	20	PECVD	X-Ray detector	[124]	
	Al ₂ O ₃	50	5	ALD	Pressure sensor	[95]	
	Al ₂ O ₃	60	30	ALD	Humidity sensor	[101]	
	Al ₂ O ₃	50	10	ALD	Photodetector	[129]	
	Al ₂ O ₃	50	10	ALD	Tactile sensor	[100]	
	HfO ₂	8–9	3	ALD	Image sensor	[94]	
	Al ₂ O ₃ /HfO ₂	40/20	3	ALD	Pressure sensor	[90]	
	Al ₂ O ₃ /SiO _x	50/10	3	ALD	Optical imager	[111]	
	(HfO ₂ /Al ₂ O ₃) ₃ /HfO ₂	(2.5/2.3) × 3 + 2.5	3.3	ALD	Magnetic sensor	[23]	
	SiO _x /Al ₂ O ₃ /SiO _x	10/20/15 0/60/10	5 10	5	ALD and e-beam deposition	Pressure sensor	[89,112]
	SiO _x /Al ₂ O ₃ /SiO _x	10/70/10	5	5	ALD and e-beam deposition	X-Ray imager	[91]
	SiO ₂ /Al ₂ O ₃	100/15 50/13	3 5	3	Thermal growth and ALD	Biosignal sensors	[26,44]
Organic dielectrics	PI	500	20	Spin coating	Pressure sensor	[64]	
	PI	750	20	Spin coating	Pressure and temperature sensor	[29]	
	PI	630	80	Spin coating	Sheet image scanner	[69]	
	PI	1000	40	Inkjet printing	Pressure sensor	[67]	
	PI	500	100–130	Inkjet printing or spin coating	Ultrasonic imager	[188]	
	SU-8	350	20	Photopatterning	X-Ray imager	[115]	
	Parylene	200	10	CVD	Pressure sensor	[66]	
Hybrid dielectrics	AlO _x /SAM	4/2	2–3	Plasma oxidation and self-assembly	Pressure sensors	[17,65,135]	
	AlO _x /SAM	4/2	2	Plasma oxidation and self-assembly	Biosignal sensor	[71]	
	AlO _x /SAM	19/2	3	Anodization and self-assembly	Pressure sensor	[18]	
	AlO _x /SAM	-/2 36/2	3 4	Anodization and self-assembly	Temperature sensors	[12,22]	
	AlO _x /SAM	20/2	5	Anodization and self-assembly	Biosignal sensor	[72]	
	Al ₂ O ₃ /Parylene	-/45	4	Plasma oxidation and CVD	Magnetic sensor	[27]	
	BaTiO ₃ and PMMA	≈3000	10	Gravure printing	Tactile sensor	[21]	
Ionic dielectrics	PEGDA and [EMIM][TFSI]	–	2 1	Photopatterning	Tactile sensors	[97,99]	
	PVDF-HFP and [EMI][TFSI]	≈150 000	3	Lamination	Pressure sensor	[81]	
	Ringer's solution or body fluid	–	0.5	–	Biosignal sensor	[20]	
	PBS solution or body fluid	–	0.5 0.4	–	Biosignal sensors	[73,74]	
Air dielectrics	Air	27 800	25	–	Pressure sensor	[98]	
	Air	21 000	15	–	Pressure sensor	[46]	

designing dielectric layers for the flexible sensory systems. Last but not least, the deposition and patterning of the gate dielectrics

should be compatible with the overall manufacturing workflow of the active matrix flexible sensors.

2.2.1. Inorganic Dielectrics

Silicon dioxide (SiO_2 , $\kappa = 3.9$) and silicon nitride (Si_3N_4 , $\kappa = 6.2$) are two typical inorganic dielectric materials intensively used in microelectronics for decades.^[110] These two dielectric materials can be employed in flexible electronics because of their facile fabrication through plasma-enhanced chemical vapor deposition (PECVD). SiO_2 and Si_3N_4 dielectric layers have been used in active matrix pressure sensors,^[45,52] photodetectors,^[24,53,54] and biosignal sensors,^[41–43] to name a few. However, due to their small κ values, relatively thick dielectric layers are necessary to meet the gate leakage limitation, which would make the TFTs brittle. In addition, a relatively high voltage is generally needed to drive these sensors.

During last decade, high- κ dielectric materials such as aluminum oxide (Al_2O_3 , $\kappa = 9.0$) and hafnium oxide (HfO_2 , $\kappa = 20\text{--}25$) have been introduced to flexible TFTs to improve their electrical and mechanical performances.^[107] Atomic layer deposition (ALD) has been applied for the fabrication of high-quality Al_2O_3 and HfO_2 films.^[86] The thickness of the Al_2O_3 and HfO_2 dielectric layers can be precisely controlled through the ALD process, and the dielectric quality is highly improved thanks to the layer-by-layer deposited dense films. The advantages of using high- κ dielectrics are twofold. First, the operation voltage can be dramatically decreased by using thinner dielectric layer. With the implementation of 8–9 nm-thick HfO_2 dielectric layer, the operation voltage of the nanowire-based image sensor can be as low as 3 V.^[94] Second, the ultrathin dielectric layer can withstand a large strain during bending and folding of the electronics, making the whole sensor devices more mechanically compliant.^[17]

Recently, combinations of different inorganic dielectric materials have been used for active matrix flexible sensors by combining the advantages of individual materials. For example, in the optical image sensors the high- κ dielectric Al_2O_3 is sandwiched between two SiO_2 layers to protect it from the alkaline resist developer.^[111] Similar $\text{SiO}_2/\text{Al}_2\text{O}_3$ hybrid dielectrics are also employed in SWCNT TFT active matrix flexible pressure sensors and X-Ray imagers, where the top SiO_2 surface is used as an adhesion layer for the SWCNTs.^[89,91,112] In our recent article, ALD-deposited $\text{HfO}_2/\text{Al}_2\text{O}_3/\text{HfO}_2$ sandwich structure is used as the dielectric layer for a-IGZO TFT active matrix by taking advantage of the large bandgap of Al_2O_3 and high dielectric constant of HfO_2 . The equivalent k value of the 6.2 nm $\text{HfO}_2/3.5$ nm $\text{Al}_2\text{O}_3/6.2$ nm HfO_2 layer is 15.3, and the a-IGZO TFT active matrix can work at a low voltage of 1.8 V.^[86] The hybrid high- k inorganic dielectric materials show great potential in the active matrix flexible sensory systems.

2.2.2. Organic Dielectrics

Besides the extensively reported inorganic dielectrics, there are some trials by using organic materials as the dielectrics for the organic semiconductor-based active matrix flexible sensors. The organic dielectrics can be facilely deposited by solution processing methods like spin coating and inkjet printing.^[31,67,68,113] Therefore, it is promising in the large-area applications of flexible

sensors. Moreover, the inherent flexibility of the organic materials can contribute to the overall compliance of the sensor devices.^[114] However, there are some obstacles for the application of organic dielectrics in high-performance active matrix flexible sensory systems. For instance, the dielectric constants of the organic materials are generally low, thus a thinner dielectric layer is required to increase the gate capacitance, thereby decreasing the operation voltage. On the other hand, a relatively large thickness is necessary to obtain pinhole-free films by the solution processed methods. Therefore, the electrical performance of the organic material-gated TFTs would be compromised by the material properties. In the pentacene OTFT active matrix pressure sensors with polyimide (PI) dielectric layers, several hundreds of nanometer thick PI films are spin-coated and the minimum operation voltage is still 20 V.^[64] Recently, pinhole-free parylene thin films with a thickness of 200 nm can be deposited by CVD, and the obtained DNNT TFT active matrix pressure sensors can be operated with voltage down to 10 V.^[66] Photopatternable SU-8 resist is also reported as gate dielectric layer for X-Ray imager,^[115] where the SU-8 layer can be directly patterned by UV light exposure without tedious plasma etching for the patterning.

2.2.3. Organic/Inorganic Hybrid Dielectrics

To further decrease the operation voltage and improve the mechanic performance of the active matrix flexible sensors, organic/inorganic hybrid dielectrics have been employed. One typical example is the combination of inorganic AlO_x and organic self-assembled monolayer (SAM).^[12,17,18,22,65,71,72] In these devices, Al metal is used as the gate electrodes, on top of which a dense AlO_x layer with a thickness down to several nanometers is generated by either plasma oxidation or anodization. Then the samples are immersed into a solution containing organic molecules with long alkyl chain such as *n*-octadecylphosphonic acid to create a densely packed organic SAM layer on the surface of the inorganic dielectric layer. The organic/inorganic hybrid dielectric layer brings the operation voltage down to 2–3 V, and the obtained DNNT TFT active matrix sensors exhibit ultraflexible and imperceptible properties, which can be folded, crumpled, and conformably attached to curved surfaces.^[18] Recently, the plasma-oxidized AlO_x is also combined with CVD-deposited parylene for the construction of active matrix magnetic sensory system with an operation voltage of 4 V.^[27]

Another motivation to use organic/inorganic hybrid dielectric materials is their ease of fabrication in large areas by solution-processed printing techniques. One successful example is the application of poly(methyl methacrylate) (PMMA) binder embedded with high- κ barium titanate (BaTiO_3) nanoparticles as the dielectric layer in SWCNT TFT active matrix tactile sensors.^[21,30,32] The dielectric ink is patterned by a gravure printing technique. The tactile sensor is with an operation voltage of 10 V due to the large thickness of the $\text{BaTiO}_3/\text{PMMA}$ patterns.^[21] The operation voltage could be further decreased by optimizing the dielectric ink formulation to obtain thinner pinhole-free films.

2.2.4. Ionic Dielectrics

Different from TFTs with solid-state dielectrics, electrolyte-gated transistors (EGTs) use a high-capacitance electrolyte as the gate dielectric material, where ions play critical roles in determining the electrical performance.^[116,117] The huge capacitance of the EGTs (typically on the order of $1\text{--}10\ \mu\text{F cm}^{-2}$) significantly lowers the device operation voltage, increases the driving current, and enables new transistor architectures. Typical electrolyte materials for the EGTs include composites that contain inorganic salts and ion coordinating polymers, ionic liquids, ion gels, polyelectrolytes, and ceramic ionic conductors, to name a few.^[118] The ionic dielectric materials have been used to construct active matrix flexible sensors such as tactile sensors, pressure sensors, and biosignal sensors. For example, the ion gel composed of poly(ethylene glycol) diacrylate (PEGDA) and 1-ethyl-3-methylimidazolium bis(trifluoromethyl sulfonyl)imide ([EMIM][TFSI]) ionic liquid has been used in graphene TFT active matrix pressure sensors.^[97,99] The operation voltage of these devices is as low as 1 V. Ion gel composed of poly(vinylidene fluoride-co-hexafluoropropylene) (PVDF-HFP) and 1-ethyl-3-methylimidazolium bis(trifluoromethylsulfonyl)amide [EM1][TFSA] has been used in intrinsically stretchable active matrix for driving rubbery tactile sensing skins.^[81]

OECT is a special kind of EGT with ion-permeable channels, where the ions in the electrolytes can be injected into the semiconductor channels and electrochemically dope the semiconductor molecules.^[78,119] In recent years, PEDOT:PSS OECTs have been widely used as multielectrode arrays for spatiotemporal bioelectrical signal detection.^[120] For the *in vitro* test of these devices, aqueous solutions such as Ringer's solution^[20] and PBS solution^[74] are considered as the gate dielectric materials. For the *in vivo* test, the body fluids are considered as the dielectrics. The operation voltage of the devices can be as low as 0.4 V.^[20]

Although the ionic dielectric materials have shown great promise in the application of various flexible sensors, the slow operation speed would be a key challenge for fast sampling applications due to the small migration rate of ions. The operation speed can be improved by decreasing the electrolyte layer thickness and using ionic liquids with fast migrating ions as the gate dielectrics.^[78]

2.2.5. Air Dielectrics

In some sensor applications, air is used as the dielectric material to construct the active matrices. For example, air dielectric-gated graphene TFT active matrix pressure sensors have been reported, where the pressure is directly transduced to the thickness variation of the air dielectric layer, thus modulating the transfer performance of the graphene TFTs.^[98] Air dielectric is also used in silicon TFT active matrix for the visualization of tactile pressures.^[46] A high operation voltage is generally needed to drive these air dielectric-based sensors due to the weak coupling of the gate electrodes to the semiconductor channels. Advanced fabrication strategies to decrease the air layer thickness would be adopted to decrease the operation voltages.

2.3. Substrate Materials

Substrate materials play a huge role in determining the overall mechanical flexibility of the active matrix flexible sensory systems.^[121,122] As listed in **Table 3**, a number of plastic films are used as substrates for the flexible sensory systems, including high transition glass temperature (T_g) polymers such as PI, and semicrystalline polyesters such as poly(ethylene 2,6-naphthalate) (PEN) and poly(ethylene terephthalate) (PET). Among these polymer substrates, PI exhibits excellent flexibility, high temperature and chemical stabilities, and low coefficient of thermal expansion. These properties make the PI substrates compatible with the photolithographic process. It needs to point out that the yellowish color of PI makes it not suitable for some applications such as in optoelectronics where high transparency is required. To address this issue, transparent PI materials have been synthesized.^[123] PEN and PET show high transparency with transmittance of $>85\%$ in the visible wavelength region. Although the thermal stability of PEN and PET is inferior to PI, they are also widely reported as substrates for active matrix pressure sensors,^[21,64,97] temperature sensors,^[12] biosignal sensors,^[71] and sheet image scanners,^[70] as well as X-Ray detectors.^[115,124] Parylene, PDMS, and SU-8 have also been reported as substrates for active matrix flexible sensory systems. The application of PDMS substrate, combining with the device geometry design or the implementation of intrinsically stretchable materials, leads to stretchable active matrix sensors.^[19,81,125,126] Recently, bioreabsorbable polymer poly(lactic-co-glycolic acid) (PLGA) have been used as substrate for transient implantable biosignal sensors.^[42]

During the last two decades, the active matrix sensor devices have evolved from flexible and ultraflexible to imperceptible and implantable. In the first demonstration of active matrix pressure sensors, the thickness of the flexible substrate is $100\ \mu\text{m}$.^[64] Nowadays, as reported in some imperceptible tactile sensors and implantable biosensors, the substrate thickness is as low as $1.2\ \mu\text{m}$.^[18] The remarkable decrease of the substrate thickness together with the adoption of neutral strain plane design principle^[37,127] has dramatically improved the device flexibility. Meanwhile, the ultrathin polymeric substrates bring some challenges from the point view of device fabrication. First, the electrical performance of the active matrices is sensitive to the surface roughness of the ultrathin substrates. Therefore, proper smoothing layer is required prior to the device fabrication.^[17] Second, the gas and moisture permeabilities have an inversely proportion to the polymer film thickness, and ultrathin polymeric substrates would inevitably suffer from deterioration of their gas barrier performance,^[76] especially for the OTFT active matrix sensors which are sensitive to oxygen and humidity, as well as for the implanted biosensors surrounded by body fluids. Thus, a good passivation or gas barrier layer is needed to improve the device stability. Third, the handling of the ultraflexible substrates would be problematic during the fabrication process. Therefore, these ultraflexible polymeric foils need to be adhered to rigid substrates before device fabrication. After the device fabrication, the flexible substrates together with the whole sensors are released from the handling substrates by various methods, such as direct peeling off, laser liftoff, and sacrificial layer-assisted delamination, as listed in Table 3.

Table 3. Typical substrate materials for active matrix flexible sensory systems.

Substrate material	Maximum temperature for substrate (°C)	Thickness (μm)	Fabrication method	Release method	Sensor type	Reference
PI	180	75	–	–	Pressure sensors	[67,19]
		12.5	–	–	–	–
	300	24	Spin coating	Peeling off	Pressure sensors	[89,95,112]
	150	75	Lamination	Peeling off	Pressure sensor	[90]
	120	100	–	–	Tactile sensor	[47]
	–	25	Lamination	Peeling off	Tactile sensor	[46]
	300	24	Spin coating	Peeling off	X-Ray imager	[91]
	300	3	Spin coating	–	Photodetector	[129]
	500	10	Spin coating	Laser liftoff	Conformable imager	[24]
	350	10	Spin coating	Delamination	Optical image sensor	[111]
	≈250	≈25	–	–	Biosignal sensor	[41]
–	13	Lamination	Peeling off	Biosignal sensors	[26,44]	
PEN	180	100	–	–	Pressure sensor	[64]
	–	1.2	Lamination	Peeling off	Pressure sensor	[18]
	190	125	–	–	Sheet image scanner	[69]
	160–170	–	–	–	X-Ray detector	[170]
	170	25	Lamination	Peeling off	X-Ray detector	[115]
	100	12	Lamination	Peeling off	Temperature sensor	[12]
	121	1.2	–	–	Biosignal sensor	[71]
PET	110	175	–	–	Temperature and pressure sensor	[189]
	150	100	–	–	Tactile sensors	[21,32]
Parylene	–	1	CVD	–	Pressure sensor	[66]
	140	2	CVD	–	Biosignal sensor	[20]
	100–140	0.6	CVD	SL-assisted delamination	Biosignal sensors	[72-74]
		1.2	–	–	–	–
–	1.2	–	–	–	–	
120	1.5	CVD	–	Magnetic sensor	[27]	
PDMS	110	–	–	–	Humidity sensor	[101]
	90	–	Spin coating	Peeling off	Tactile sensor	[81]
–	–	27.8	Spin coating	SL-assisted delamination	Pressure sensor	[98]
SU-8	–	1.5	Spin coating	SL-assisted delamination	Tactile sensor	[100]
PLGA	55–60	≈30	–	–	Biosignal sensor	[42]

It is envisioned that the flexibility of the active matrix sensors can be further improved by selecting proper substrate materials and decreasing the thickness of the substrate down to the sub-micrometer range. Moreover, substrate-free breathable sensor devices could be fabricated and directly attached to the human skins as electronic tattoos.^[128]

3. Pixel Design for the Active Matrix Flexible Sensory Systems

The active matrix flexible sensory systems are composed of identical TFT-driven sensor pixels which are distributed over a large area for local signal detection. To realize reliable signal readout with high spatiotemporal resolution, the pixel circuits

need to be carefully designed. **Figure 4** shows some typical circuit diagrams of single pixels in the currently reported active matrix flexible sensory systems. Among them, the simplest design is using one TFT as the multiplexer for pixel selection and one sensing element in serial connection with the control TFT. The sensing elements can be resistor-type, such as piezoresponsive resistors for pressure sensors^[64] and thermistors for temperature sensors^[12] (Figure 4a), diode-type, such as photodiodes for image sensors (Figure 4b),^[49] and transistor-type, such as OECTs for local electrophysiological signal recording and amplification (Figure 4d).^[72] In some user-interactive flexible sensors, LEDs have been serially connected into the pixels together with the sensing elements, which can indicate the measured signals through the variation of their emission intensity (Figure 4c).^[89]

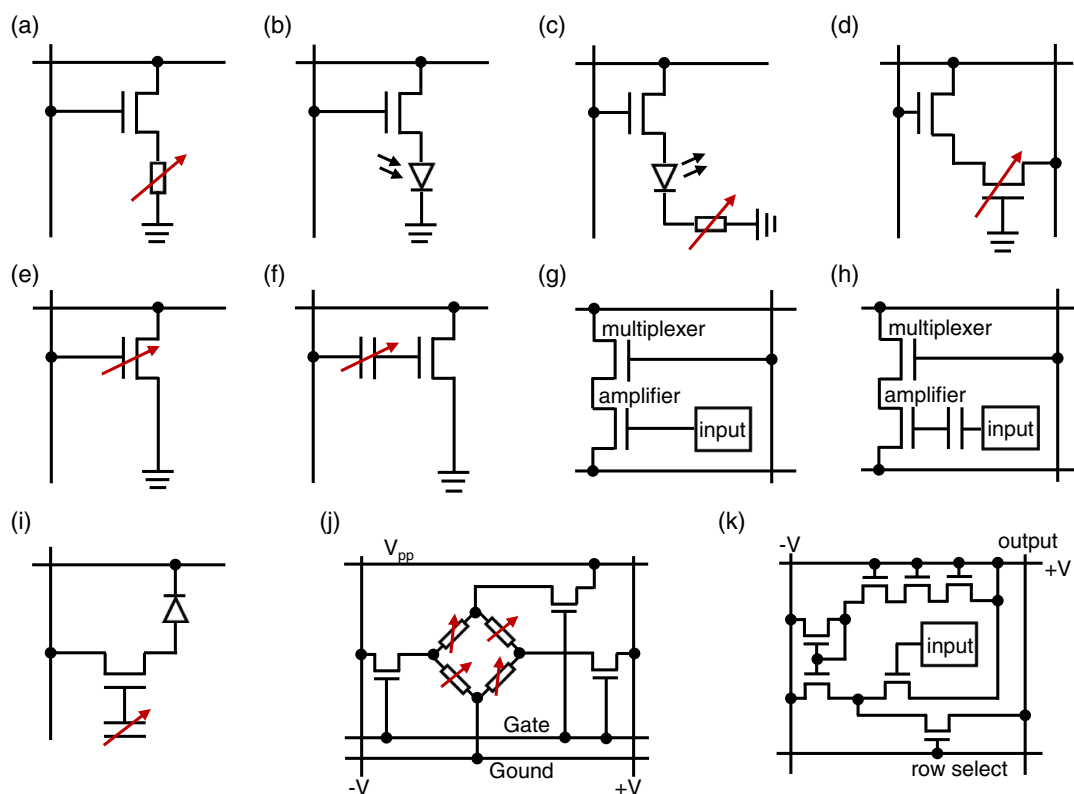


Figure 4. Summary of some reported pixel designs for the active matrix flexible sensory systems. a) A resistor-type sensor is in serial connection with the control TFT. Adapted with permission.^[12] Copyright 2016, Wiley-VCH Verlag GmbH & Co. KGaA. b) A diode-type sensor is in serial connection with the control TFT. Adapted with permission.^[49] Copyright 2008, American Institute of Physics. c) A resistor-type sensor and a LED are serially connected into the pixel. Adapted with permission.^[89] Copyright 2013, Macmillan Publishers Ltd. d) A transistor-type sensor is in serial connection with the control TFT. Adapted with permission.^[72] Copyright 2016, Wiley-VCH Verlag GmbH & Co. KGaA. e) The TFT functions both as the multiplexer and the sensor. Reproduced under the terms of the CC BY license.^[98] Copyright 2017, The Authors. Springer Nature. f) A capacitor-type sensor is connected to the gate electrode of the control TFT. Adapted with permission.^[99] Copyright 2015, Wiley-VCH Verlag GmbH & Co. KGaA. g) Conductively coupled signal input design. Adapted with permission.^[44] Copyright 2018, The Authors. Published under the PNAS license. h) Capacitively coupled signal input design. Adapted with permission.^[26] Copyright 2017, Macmillan Publishers Ltd., part of Springer Nature. i) Tribotronic transistor as the sensor element. Adapted with permission.^[47] Copyright 2016, American Chemical Society. j) Wheatstone bridge configuration design for differential signal readout.^[23] Copyright 2022, The Authors. Published by Springer Nature. k) The amplifiers are integrated into the pixels. Adapted with permission.^[41] Copyright 2010, American Association for the Advancement of Science.

The current modulation capability of the TFT is dependent on the capacitance coupling between the gate and the semiconductor channel, which can be tuned by external stimuli. Therefore, in some reported graphene TFT active matrix pressure sensors and PEDOT:PSS OECT-based multielectrode arrays, the TFTs function both as multiplexers and sensors, as shown in Figure 4e.^[20,98] In this configuration, the input signals from the gate electrodes could be amplified owing to the current modulation of the TFTs. To take advantage of the signal amplification property of the TFTs, the sensor elements could also be connected to the gate electrodes of the control TFTs, as shown in Figure 4f. For example, piezoelectric nanogenerators have been coupled to the gate of graphene TFTs to realize active matrix strain sensors.^[99] Recently, the tribotronic transistors have been reported as sensor pixels for active tactile sensing system, where the tribotronic transistors are gated by external stimuli, acting as sensing elements by virtue of the change of the source–drain

current (Figure 4i).^[47] The serially integrated diode ensures the current flows through the TFTs in only one direction.

Figure 4g,h demonstrates pixels with more complex designs with one multiplexing TFT and one sensing unit. In the sensing unit, the signal input terminal is connected to the gate of an amplifying TFT through conductive (Figure 4g)^[44] or capacitive coupling (Figure 4h).^[26] In these kinds of designs, the multiplexing and amplifying TFTs are independent with each other. Therefore, the TFT geometries could be individually designed to meet specific requirements. Thanks to the in-pixel integrated amplifiers, the electrophysiological signals can be read out with high fidelity. As shown in Figure 4k, more complex amplifying circuits have also been integrated into single pixels for the detection of weak biosignals. The amplifier uses a source-follower configuration with current gain.^[41] Recently, we have proposed a novel pixel design with Wheatstone bridge configuration for the driving and signal readout of

magnetoresistance-type sensors (Figure 4j).^[23] The pixel has one Wheatstone bridge anisotropic magnetoresistance (ARM) sensor, one driving TFT and two readout TFTs. The three TFTs in the pixel share the same gate line, thus can be activated synchronously. Differential voltage signals are picked up in a parallel way, leading to fast signal readout and small crosstalk.

In addition to the typical pixel circuits listed above, there are also some other pixel designs reported in flexible sensor applications. For example, active matrix of nonvolatile memory TFTs with floating gates have been integrated with pressure sensitive resistors to construct flexible pressure sensor arrays.^[65] The spatial distribution of mechanical pressure can be stored and retrieved after removal of the pressure and voltages. Recently, in-pixel charge integrating circuit has been used in a-IGZO TFT active matrix photodetector arrays to discriminate different colors.^[129]

As various kinds of pixel configurations have been proposed for the active matrix flexible sensory systems, the main purpose of the pixel design is the same: to extract high-fidelity signals with high spatiotemporal resolution. Therefore, several principles could be summarized for the design of the sensor pixels. First, the pixels should be designed as simple as possible to realize the equivalent functions because complex design will inevitably increase the fabrication price and decrease the overall yield. As a result, sometimes the final design is the compromise between the system sophistication and the device performance. Second, the layouts of the pixels need to meet the requirement of the spatial resolution for the sensor arrays. Third, for large-area sensor arrays with multiple channels, the sampling speed needs to be taken into consideration by adopting, for instance, parallel readout to ensure the real-time signal monitoring. Last but not least, the yield of the pixels has to be considered because small defects are hardly to avoid in large-area device fabrication. To address this issue, redundant design is suggested for the improvement of the overall yield for the devices. Another option is to electrically isolate the dysfunctional pixels from the whole system to avoid their influence on other working pixels. With the advances in active matrix flexible sensory systems, other pixel configurations with various applicable functionalities will be promoted which can greatly simplify the device fabrication and broaden the sensor application.

4. Typical Fabrication Methods for the Active Matrix Flexible Sensory Systems

During the last decades, the motivation for producing large-area, high-definition flat panel displays has driven the advances of conventional microfabrication technologies for active matrix backplanes on rigid substrates.^[130] Although many of the well-developed fabrication toolkits in modern semiconductor technologies, such as photolithography, metallization, wet, and dry etching techniques, can be transferred to the fabrication of active matrix flexible sensors, the whole integration strategies leading to high-performance flexible sensory systems need to be adjusted by considering the flexible form factor of the devices and the special material combinations used for the TFT backplanes and the sensors. Moreover, low-cost large-area manufacturing of the active matrix flexible sensors is required for their scalable applications. As illustrated in Figure 5, state-

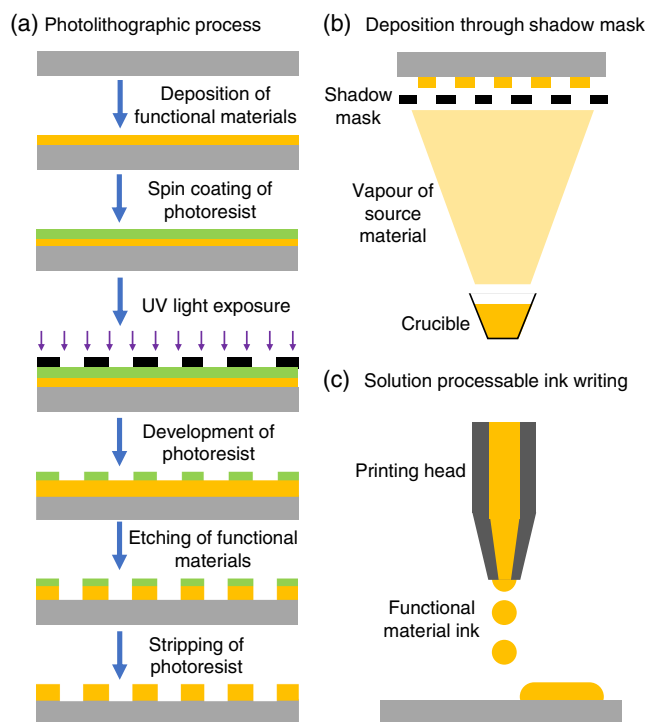


Figure 5. Illustration of typical fabrication methods to construct active matrix flexible sensors. a) Illustration of photolithographic process. b) Illustration to show the deposition of functional material patterns through a shadow mask. c) Illustration of inkjet printing as a typical solution processable ink-based direct writing technique.

of-the-art fabrication strategies for the active matrix flexible sensory systems mainly include photolithography, shadow mask-assisted deposition, solution processable ink-based printing technologies, and hybrid methods that combine different fabrication approaches.

4.1. Photolithographic Process

Photolithography is one of the mainstream fabrication technologies for high-performance active matrix flexible sensory systems.^[28,129] The typical steps for photolithography are schematically illustrated in Figure 5a. It is a subtractive process, where the functional materials are deposited covering the whole surface of the substrate and then etched to defined patterns with the assistance of photoresists.^[131] High-resolution features down to the nanometer scale can be obtained by this process, at the expense of multiple steps including the spin coating of photoresists, UV light exposure, development, and stripping of the photoresists. Functional materials can be integrated in a layer-by-layer manner with excellent pattern registration by repeating the photolithographic process. Although photolithography provides precise control of the material patterns, there are some challenges when it is applied to the fabrication of active matrix flexible sensory systems. First, a flat substrate is required for transferring the patterns from the hard masks to the functional material thin films with high fidelity. To meet this requirement, flexible substrates have to be attached to flat rigid handling

substrates during the fabrication and the obtained devices are released from the substrates after fabrication, which generates additional steps.^[34–36] Second, aqueous and organic solvents are frequently used during the photolithographic process. However, many functional materials for active matrix flexible sensory systems, such as the organic semiconductor channel materials and the sensor transducing materials, are sensitive to moisture and solvents.^[28] Therefore, additional passivation steps are necessary. Although with these limitations, photolithography will be still one of the main fabrication technologies for high-performance active matrix flexible sensory systems.

4.2. Shadow Masking Technique

Shadow masking technique (stencil lithography) is a resistless material patterning and thin-film device fabrication method, in which the source materials can be evaporated and deposited onto target substrates through shadow masks (Figure 5b).^[132,133] The process can be carried out in totally dry condition because the photoresist-related wet chemistry is avoided. Therefore, it is quite suitable for the integration of materials that are sensitive to moisture and solvents.^[134] The shadow masking technique has been widely applied for the fabrication of OTFT active matrix flexible sensors. Two typical organic semiconductors, namely, pentacene^[29,64,65,69] and DNNT,^[18,71,135,136] have been deposited as the channel materials through shadow masks. The obtained OTFT active matrices demonstrate excellent electrical performance and are used for driving different flexible sensor arrays. It needs to point out that although shadow masking technique

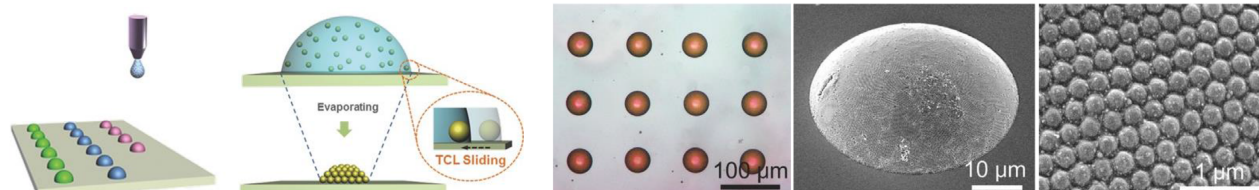
eliminates multiple steps as required for photolithographic process, it suffers from low pattern resolution and nonideal layer registration. High precision alignment systems combined with ultrafine shadow masks will be a solution to these limitations.

4.3. Solution Processable Ink-Based Printing Technologies

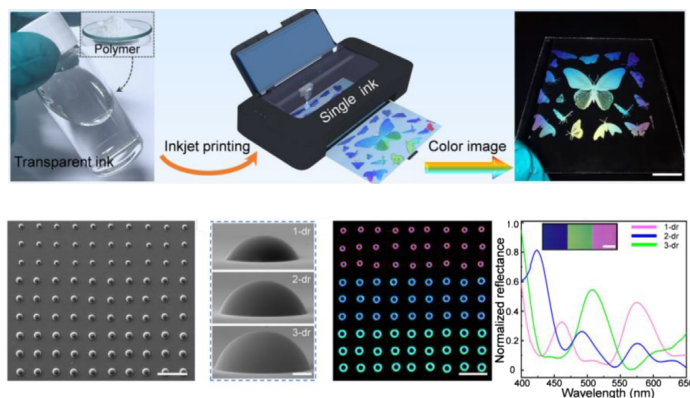
In recent years, solution processable ink-based printing technologies have been intensively explored for the fabrication of flexible and printed electronics.^[137–140] Different from subtractive photolithographic process, the additive printing techniques directly deposit functional material inks onto the substrates for constructing microelectronic devices.^[141–144] The selective deposition of solution processable materials can reduce the fabrication cost, eliminate the vast waste of solvents, and enable large-area manufacturing.^[68] Furthermore, this process is capable of fabricating devices on soft, flexible, and nontraditional substrates in a roll-to-roll manner.^[63] Due to these advantages, the solution processable ink-based printing technologies, such as inkjet printing (Figure 5c),^[145,146] transfer printing,^[16] screen printing,^[147] gravure printing,^[63] and roll-to-roll printing,^[32,148,149] have been employed for the fabrication of various active matrix flexible sensory systems.

Among the solution-processed ink-based printing technologies, the digital inkjet printing technique has caught great attention because it offers a versatile and low-cost methodology to integrate diverse functional materials on the same chip by designing the ink formulations, the substrate wettability, and the printing manners.^[150–152] Figure 6 shows several examples

(a) Inkjet printing and assembly of PC dome patterns (b) QD-PC nanocomposite patterns by reactive inkjet printing



(c) Full-color inkjet printing with a single transparent ink



(d) Multilayer circuits fabricated by inkjet printing

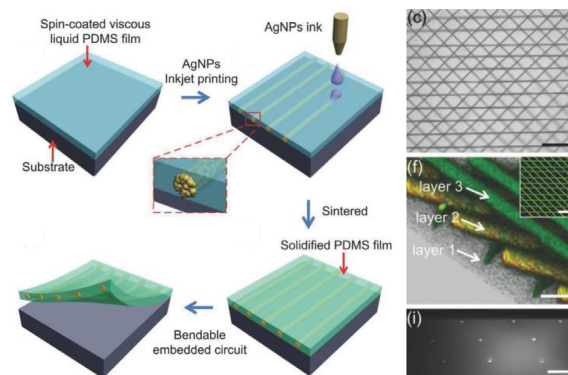


Figure 6. Solution processed inkjet printing technology for the integration of functional materials. a) Illustration showing the inkjet printing and self-assembly of the colloidal PC dome patterns. Reproduced with permission.^[153] Copyright 2013, The Authors. Published by Wiley-VCH. b) Photograph and SEM images of the QD-PC nanocomposite patterns fabricated by reactive inkjet printing. Reproduced with permission.^[154] Copyright 2015, Wiley-VCH. c) Full-color inkjet printing with a single transparent ink. Reproduced with permission.^[155] Copyright 2021, The Authors. Published by AAAS. d) Multilayer circuits fabricated by inkjet printing. Reproduced with permission.^[156] Copyright 2015, The Authors. Published by Wiley-VCH.

of the applications for the inkjet printing in material integrations. Figure 6a demonstrates the illustration for the inkjet printing and self-assembly of colloidal photonic crystal (PC) dome patterns.^[153] Dome shaped, self-assembled colloidal microstructures are realized by controlling the interaction between the printed ink and the substrate. The obtained PC dome array has a wide viewing angle from 0° to 180° when the fluorescent molecules are incorporated. Similar quantum dot (QD)-PC hybrid nanocomposite dome-structured arrays are obtained by reactive inkjet printing (Figure 6b).^[154] The fluorescent QD nanocrystals are in-situ generated by combining the printing of their solution precursors and subsequent gas treatment. Recently, a structural-color printing approach has been proposed to achieve full-color integration of high-photorealistic images from a single transparent ink (Figure 6c).^[155] Microdomes with different sizes can be facily integrated on the same substrate by controlling the substrate wettability and the printed ink volumes. The microscale concave interface results in total internal reflection of the incident lights, thus vivid structural colors covering the whole visible light range are obtained depending on the size of the microdomes. Furthermore, exquisite structural-color images can be realized by heterogeneous integration of microdomes with different sizes. These inkjet-printed photonic microstructures would find numerous applications when they are integrated within the flexible active matrices for optoelectronic sensors. In addition to the inkjet printing of photonic devices, the inkjet printing technique is also extensively used to fabricate electronic devices. For example, flexible multilayer circuits can be fabricated in a layer-by-layer printing manner (Figure 6d).^[156] In the multilayer circuits, the conductive sliver nanoparticle (Ag NP) inks are inkjet-printed and embedded into transparent flexible polydimethylsiloxane (PDMS) films. The resolution of the printed Ag

cables is highly improved due to the suppression of the ink spreading by the viscous PDMS substrate. Meanwhile, the transparency and flexibility of the circuits are improved owing to the wrapping of the Ag cables within the PDMS substrates. The inkjet-printed multilayer circuits would find potential applications for the interconnects in the active matrix flexible sensory systems.

Figure 7 shows typical active matrix backplanes fabricated by printing technologies. The first reported large-area flexible OTFT active matrix backplane is fabricated by microcontact transfer printing (Figure 7a).^[16] The on-current of the OTFTs can reach several microamperes, which is high enough to switch on the pixels of the electrophoretic electronic paper. Although the active matrix backplane was demonstrated for driving displays, it has promoted the development of printable active matrix flexible sensors. SWCNT is a promising semiconductor channel material that enables solution processability for large-area flexible electronics. Figure 7b shows the SWCNT TFT active matrix backplane fabricated by inverse gravure printing.^[30] In this backplane, the essential components including the gate and source/drain electrodes, the gate dielectric layer, and the SWCNT channel are fully printed in a layer-by-layer way, and the obtained SWCNT TFTs show highly uniform electrical performance, with mobility and on/off ratio of up to $\approx 9 \text{ cm}^2 \text{ V}^{-1} \text{ s}^{-1}$ and 10^5 , respectively. In addition to SWCNT TFTs, large-area and ultra-flexible OTFT active matrix backplane has also been manufactured by fully printing technique, as shown in Figure 7c.^[31] The component OTFTs in the active matrix have an average mobility of $0.7 \text{ cm}^2 \text{ V}^{-1} \text{ s}^{-1}$ and on/off ratio larger than 10^5 at operation voltages of $V_{GS} = V_{DS} = -10 \text{ V}$. The fully printing fabrication of high-performance active matrix backplanes paves the way for their board applications in large-area flexible sensory systems.

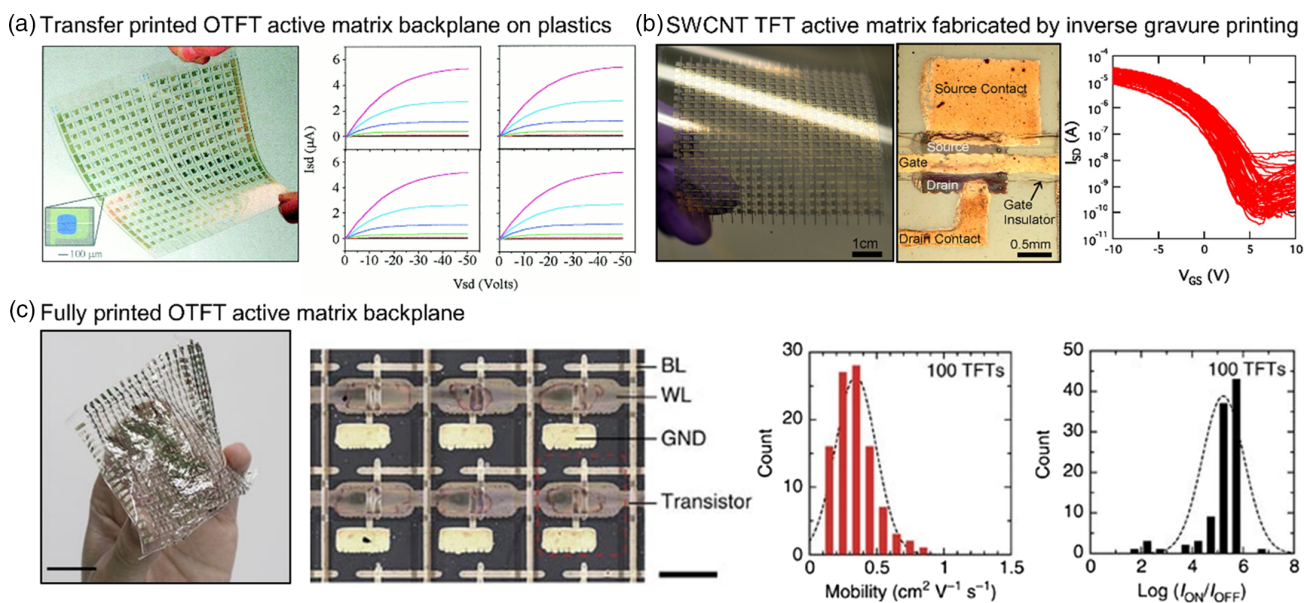


Figure 7. Active matrix backplanes fabricated by printing technologies. a) Image of a plastic active matrix backplane circuit constructed by transfer printed OTFTs and the output characteristics of several typical TFTs. Adapted with permission.^[16] Copyright 2001, National Academy of Sciences. b) Photograph, optical micrograph, and transfer characteristics of flexible SWCNT TFT active matrix fabricated by inverse gravure printing. Adapted with permission.^[30] Copyright 2013, American Chemical Society. c) Photograph, magnified view of OTFT arrays and electrical performance of OTFT active matrix fabricated by fully printing processes on parylene-C films. Adapted with permission.^[31] Copyright 2014, Macmillan Publishers Ltd.

The solution processable ink-based printing technologies have provided tremendous opportunities for flexible and wearable electronics. However, there are some issues to address for the further improvement of the printed active matrix flexible sensory systems. First, the uniformity and quality of the printed thin films are generally inferior to their counterparts obtained by vacuum depositions. Second, the resolution of the printed patterns is lower than that obtained from photolithography. Third, the material compatibility sometimes would be a problem for multi-layer printing. Nevertheless, the solution processable ink-based printing approach will continue to evolve as one of the most important complementary technologies to photolithography and will build the foundations for the next-generation electronics.

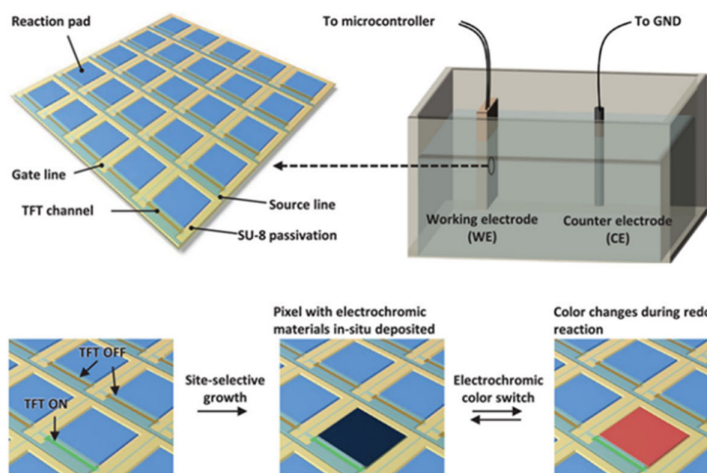
4.4. Hybrid Methods

Hybrid methods which combine the abovementioned techniques are often adopted by merging the advantages of each

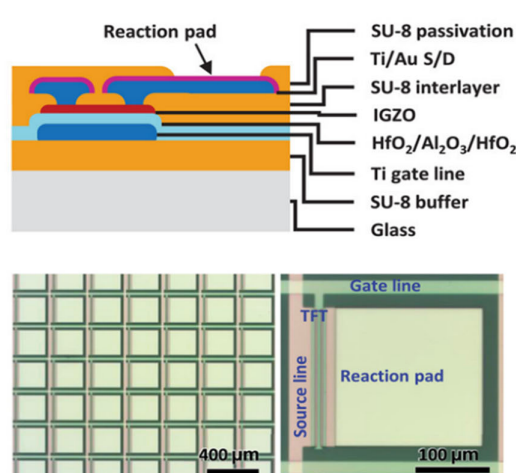
methods.^[157–159] For example, the semiconductor SWCNTs and Ge/Si nanowires are synthesized on their growth substrates and then transfer-printed to flexible substrates, which is followed by photolithographic process for device fabrication.^[90,94,95] Photolithographically obtained active matrix backplanes have been seamlessly integrated with solution deposited sensor layers for photodetector arrays,^[160] thermal imagers,^[161] and pyroelectric sensors.^[162] Shadow masking technique has been combined with photolithography in the fabrication of OTFT active matrix flexible sensors.^[22]

Recently, a digital electrochemical deposition method is proposed to in situ deposit functional materials onto the pixels controlled by photolithographically obtained a-IGZO TFT active matrix (Figure 8).^[86] The concept of the digital electrochemistry approach is illustrated in Figure 8a. The a-IGZO active matrix is used as the working electrode, where functional materials can be site-selectively deposited on the pixels by addressing the control a-IGZO TFTs. The structure of the a-IGZO active matrix is shown in Figure 8b. The reaction pad is connected to the drain of the control a-IGZO TFT, and site-selective electrochemical

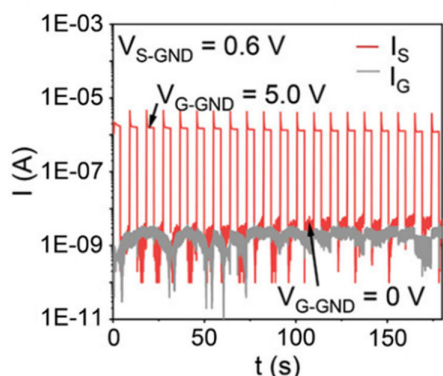
(a) Concept of the digital electrochemistry approach



(b) Structure of the a-IGZO TFT active matrix



(c) On-off operation of the TFT in solution



(d) Heterogeneous material integration by the digital electrochemistry approach

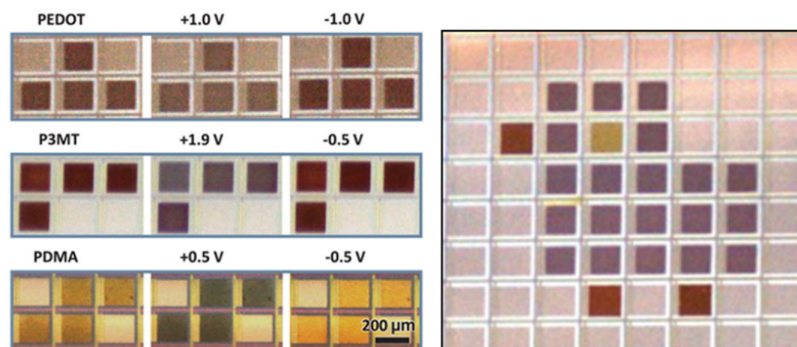


Figure 8. Digital electrochemistry approach for the heterogeneous material integration on the active matrix platform. a) Concept of the digital electrochemistry approach. b) Structure of the a-IGZO active matrix backplane. c) Currents change with time for the on-off operation of the a-IGZO TFT in the precursor aqueous solution. d) Micrographs showing the site-selective deposition of heterogeneous materials controlled by the digital electrochemistry approach. Reproduced under the terms of the CC BY license.^[86] Copyright 2021, The Authors. Published by Wiley-VCH.

reaction can take place on the reaction pad when the control TFT is switched on. The source current change during the on–off operation of the TFT in the deposition solution indicates that the electrochemistry process can be efficiently controlled through the switching of the control TFTs (Figure 8c). Monochromatic and multicolored conducting polymer patterns can be obtained by the site-selective digital electrochemistry approach, which shows its potential applications in the heterogeneous integration of multiple sensing elements on the same active matrix (Figure 8d).

The hybrid methods can broadly expand the material compatibility, which is essential for the integration of dissimilar materials. Furthermore, a balance between the fabrication price and the device performance will be achieved by employing hybrid methods for the sensor fabrication.

5. Applications of Active Matrix Flexible Sensory Systems

The active matrix backplanes have been integrated with sensing elements to construct flexible, imperceptible, and implantable sensors. Recently, the stretchable active matrix sensors have been developed based on geometric design or intrinsically stretchable materials.^[19,80–83] In this section, the applications of flexible, imperceptible, and implantable active matrix sensory systems will be reviewed, with a focus on the pressure sensors, temperature sensors, photodetectors, magnetic sensors, and biosignal sensors.

5.1. Pressure Sensors

Artificial e-skins that can recognize tactile information are essential for the robotic and prosthetic applications.^[163] By equipping with active matrix pressure sensors, the e-skins are capable of accurately perceiving spatially distributed tactile stimuli. The active matrix pressure sensors are constructed with different material combinations and device configurations. For example, OTFTs,^[18,64,66,68] nanotube/nanowire TFTs,^[21,32,89,90,95,112] and graphene TFTs^[97,99] have been used to build the active matrix backplanes. Meanwhile, traditional TFT structures as well as air and electrolyte gating have been adopted for the transistor architectures.^[97,98]

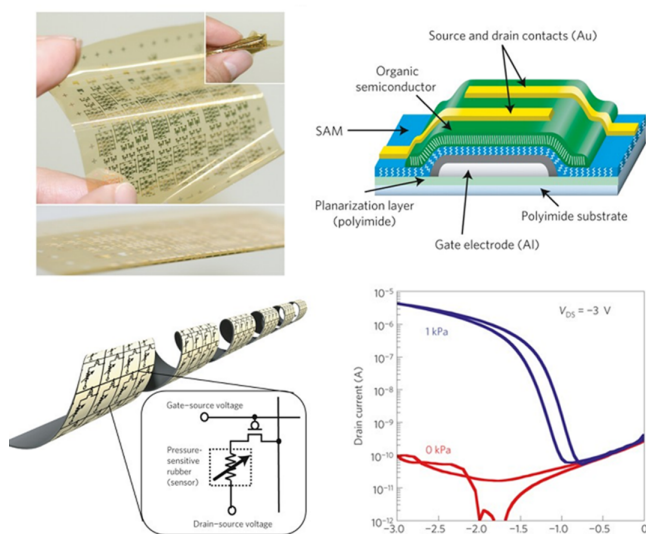
Figure 9 shows the typical OTFT active matrix flexible pressure sensors.^[17,18,66] Organic semiconductors such as pentacene and DNTT are deposited through shadow masks as the channel materials to construct the OTFT active matrix backplanes. Meanwhile, ultrathin hybrid AlO_x/SAM gate dielectric layers are adopted to decrease the operation voltage and increase the device flexibility. The OTFT active matrices are integrated with pressure-sensitive rubber sheets for the mapping of pressure distribution. As shown in Figure 9a, the ultraflexible pressure sensor can work in a tightly wound state for catheters. The applied pressure creates a conducting path through the source of the OTFTs to the pressure-sensitive rubber and then to the grounded counter electrode, thus the pressure distribution can be obtained by interrogating the OTFTs in the active matrix array.^[17] Imperceptible OTFT active matrix pressure sensor is fabricated by using a 1.2 μm -thick PEN as substrate and an 800 nm-thick

polyethylene film as encapsulation layer (Figure 9b).^[18] The OTFTs show unprecedented mechanical stability with the ultrathin design and the usage of the robust dielectrics. The OTFT active matrix can withstand repeated bending to radii of 5 μm and less, and can be crumpled like paper. The OTFTs have an average on/off ratio larger than 10^7 , which ensures the unambiguous distinction between on and off pixels. The OTFT active matrix pressure sensor can detect the profile of a metallic ring placed on top of it, with a change of TFT drain currents by more than six orders of magnitude between the contacted and noncontacted pixels. The OTFT active matrix backplane is further integrated with composite nanofibers of CNTs and graphene to fabricate bending-insensitive pressure sensors (Figure 9c).^[66] With the incorporation of the nanoporous composite nanofibers that exhibit an extremely small sensitivity to the bending-induced strain, this pressure sensor can precisely measure the distribution of the normal pressure without detecting the pressure signals from wrinkling and twisting deformations.

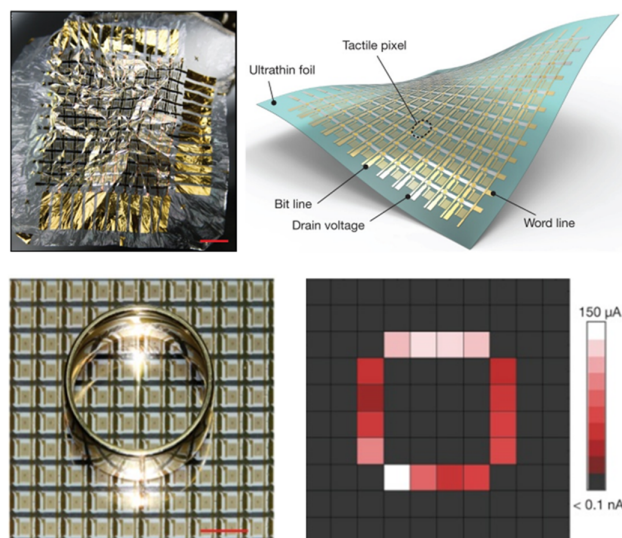
Semiconducting nanowires and nanotubes can be used as channel materials to construct high-performance active matrix pressure sensors by taking advantage of the high carrier mobilities and excellent mechanical flexibility of the 1D nanomaterials (Figure 10).^[21,89,95] As shown in Figure 10a, uniform assembly of ordered Ge/Si core/shell nanowire arrays is realized by transfer printing of the nanowires grown by vapor-liquid-solid method. Then, TFT active matrix consisting of 19×18 pixels with an active area of $7 \times 7 \text{ cm}^2$ is fabricated by standard photolithography.^[95] The pressure sensor is achieved by laminating the nanowire TFT active matrix backplane with a silicone-based pressure sensitive rubber, which can map the pressure distribution applied by a PDMS mold. To obtain user-interactive e-skins for instantaneous pressure visualization, organic LEDs are integrated into the pixels in the SWCNT TFT active matrix pressure sensory system (Figure 10b).^[89] The sensors can spatially map the pressure distribution through the change of the TFT drain currents, meanwhile the monolithically integrated LEDs can indicate the magnitude of the applied pressure though changing the intensity of their light emission. Recently, large-area SWCNT TFT active matrix backplanes have been realized by solution-based roll-to-plate gravure printing, and the obtained backplanes are integrated in tactile sensors for large-area pressure mapping (Figure 10c).^[21] When laminated with a pressure sensitive rubber, the SWCNT TFTs show different transfer characteristics depending on the amount of the applied pressure. The detectable pressure ranges from $\approx 1 \text{ kPa}$ to 20 kPa, and the linear sensitivity is $\approx 800\% \text{ kPa}^{-1}$.

Graphene, as one of the most studied 2D materials, has been used as channel material for active matrix flexible pressure and strain sensors.^[97–99] As discussed in the materials section, the graphene TFTs have huge electron and hole mobilities but cannot be totally switched off.^[102] Due to its unique material properties, special device architectures are frequently adopted when graphene is integrated in pressure sensors (Figure 11). Figure 11a shows an air-dielectric graphene TFT active matrix pressure sensor array, where local air gaps are used as the dielectrics for the top-gated graphene TFTs.^[98] The height of the air gap is decreased when external pressure is applied; thus, the capacitance of the metal–air–graphene structure is increased. The pressure-sensitive capacitance change enables the graphene

(a) Ultraflexible OTFT active matrix pressure sensor



(b) Imperceptible OTFT active matrix pressure sensor



(c) Bending-insensitive OTFT active matrix pressure sensor

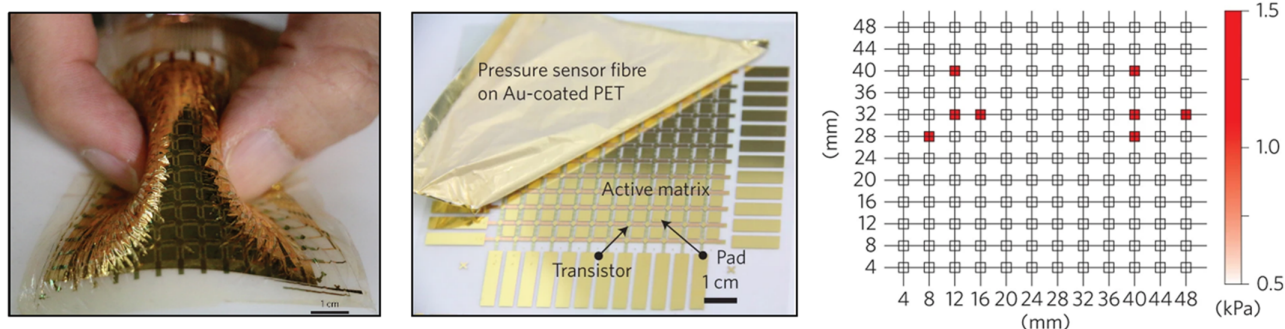


Figure 9. OTFT active matrix flexible pressure sensors. a) Ultraflexible OTFT active matrix pressure sensor. The component OTFTs show extremely bending stability even in the shape of a tightly wound helix. Adapted with permission.^[17] Copyright 2010, Macmillan Publishers Ltd. b) Imperceptible OTFT active matrix pressure sensor. The devices are ultraflexible and can be crumpled like a sheet of paper. The pressure sensor sheet can detect the profile of the metallic ring placed on top of it with a change of TFT drain currents by more than six orders of magnitude between the contacted and noncontacted pixels. Adapted with permission.^[18] Copyright 2013, Macmillan Publishers Ltd. c) Bending-insensitive OTFT active matrix pressure sensor. The OTFT active matrix is integrated with composite nanofiber sensors to only measure the normal pressure under complex bending state without showing the pressure signal from deformation. Adapted with permission.^[66] Copyright 2016, Macmillan Publishers Ltd.

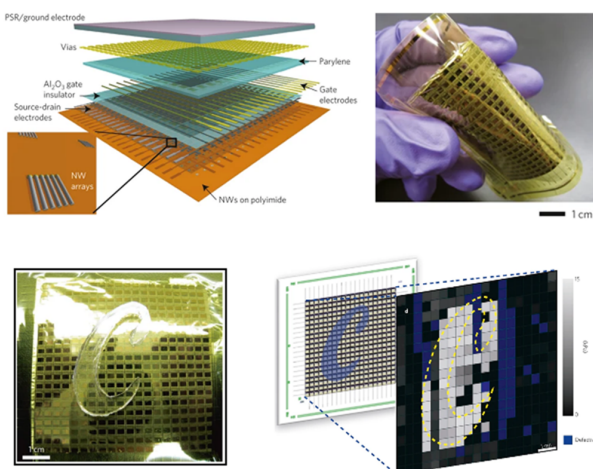
TFTs to act as tactile pressure sensors. With this unconventional structure design, the pressure sensors show a wide tactile pressure sensing range from 250 Pa to ≈ 3 MPa. In another report, the piezoelectric nanogenerators are coupled to the gate electrodes of the coplanar-gate structured graphene TFTs for active matrix strain sensors (Figure 11b).^[99] The external strain-induced piezopotentials can be effectively coupled to the TFT channels through the ion gel gate dielectric, leading to a charge accumulation in the graphene channels and thus the change of the drain currents. The strain sensors demonstrate a gauge factor of 389 and a minimum detectable strain of 0.008% with an extremely low operation voltage of 0.1 V.

5.2. Temperature Sensors

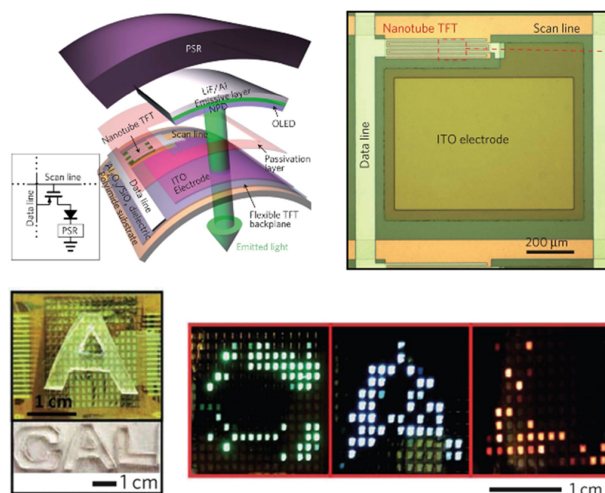
Temperature sensing modality is another important function for e-skins.^[29] The e-skins equipped with temperature sensors can

perceive the surrounding thermal conditions and the heat generated from human body.^[4] Moreover, spatiotemporal measurement of localized temperature changes in soft tissues is important in understanding the thermal phenomena of homeostasis and enabling real-time temperature monitoring during surgery.^[164] Active matrix flexible temperature sensors have been fabricated by integrating active matrices with thermistors (Figure 12). As shown in Figure 12a, flexible organic temperature sensor with 16×16 pixels is constructed by integrating DNNT TFT active matrix backplane with Ag nanoparticle/pentacene thin film thermistors.^[12] The temperature sensor exhibits a wide sensing range from 20 to 100 $^{\circ}$ C, with a temperature resolution of 0.4 $^{\circ}$ C. The temperature sensor can be conformally attached to the surfaces of various objects and the human body for temperature mapping. Figure 12b demonstrates an OTFT active matrix physiological temperature sensor with a 12×12 pixel array.^[22] The temperature sensor is fabricated by integrating DNNT

(a) Ge/Si NW TFT active matrix pressure sensor



(b) CNT TFT active matrix user-interactive pressure sensor



(c) Large area printed CNT TFT active matrix tactile sensor

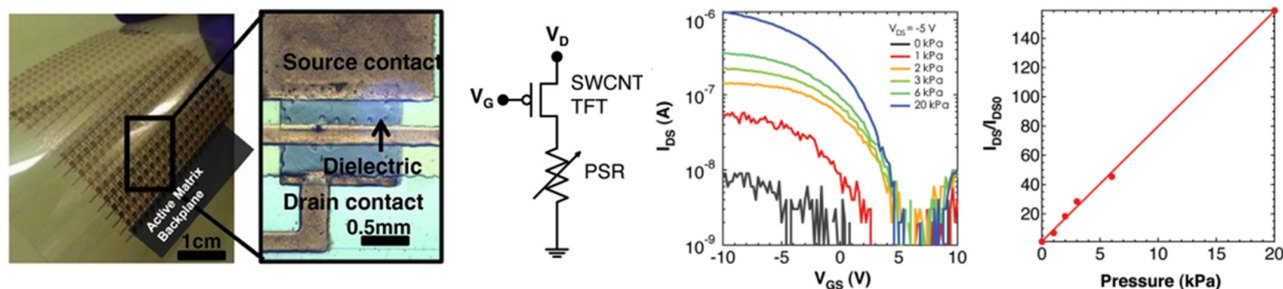


Figure 10. Nanowire and nanotube TFT active matrix pressure sensors. a) Ge/Si nanowire TFT active matrix pressure sensor. The parallel Ge/Si nanowire arrays are integrated as the active matrix backplane for flexible pressure sensors. Adapted with permission.^[95] Copyright 2010, Macmillan Publishers Ltd. b) SWCNT TFT active matrix user-interactive pressure sensor. Organic LEDs and pressure sensitive rubber are integrated with the SWCNT TFT active matrix to provide an instantaneous visual response to the magnitude of the applied pressure. Adapted with permission.^[89] Copyright 2013, Macmillan Publishers Ltd. c) Large-area printed SWCNT TFT active matrix tactile sensor. The printed SWCNT TFT active matrix backplane is integrated with tactile sensor arrays for large-area pressure mapping. Adapted with permission.^[21] Copyright 2015, Wiley-VCH Verlag GmbH & Co. KGaA.

TFT active matrix backplane with a highly temperature-sensitive composite composed of graphite particles and acrylate copolymers. The detectable temperature ranges from 25 to 50 °C, with a sensitivity of 0.1 °C or less, and the response time is as fast as 100 ms. Thanks to its superb mechanical flexibility, the sensor can be compliantly attached to the lung surface for in vivo temperature mapping during very fast artificial respiration. Besides the flexible OTFT active matrix temperature sensors, stretchable active matrix temperature sensor array integrated with SWCNT TFT backplane and polyaniline nanofiber sensor elements has also been reported.^[165] The adoption of liquid metal galinstan interconnects enables the sensor to be mechanically stable under a biaxial stretching of 30%. The sensing temperature ranges from 15 to 45 °C with a resistance sensitivity of 1.0% °C⁻¹, and the sensor response time is 1.8 s.

5.3. Photodetectors and Imagers

In recent years, the demands for large-area flexible photodetectors and imagers are increasing, particularly for medical and

security applications.^[160,166–168] Flexible photodetectors can be directly attached to the human skins, allowing continuous monitoring of vital signs.^[129] Sheet image scanners that are based on flexible photodetector arrays have no moving parts and do not require any optics, thus can be broadly used in human-friendly mobile electronics.^[69]

Figure 13 demonstrates some reported active matrix flexible photodetectors.^[24,49,69,94,160] In these photodetectors, photosensor elements such as photoconductors, photodiodes, and phototransistors have been integrated with the active matrix backplanes. Figure 13a shows the photograph and pixel circuit diagram of an a-Si:H TFT active matrix image sensor.^[49] Organic photodiodes composed of poly[2-methoxy-5-(2-ethylhexyloxy)-1,4-phenylene-vinylene] and [6,6]-phenyl-C61-butyric acid methyl ester (MEHPPV-PCBM) bulk heterojunction are used as the sensor elements. The image sensor consists of 180 × 180 pixels with a resolution of 75 dots per inch (dpi). Figure 13b shows the photograph and layer stack illustration of an OTFT active matrix sheet image scanner.^[69] A 30 nm-thick p-type semiconductor copper phthalocyanine (CuPc) and a

(a) Air-dielectric graphene TFT active matrix pressure sensor

(b) Piezopotential-powered graphene TFT active matrix strain sensor

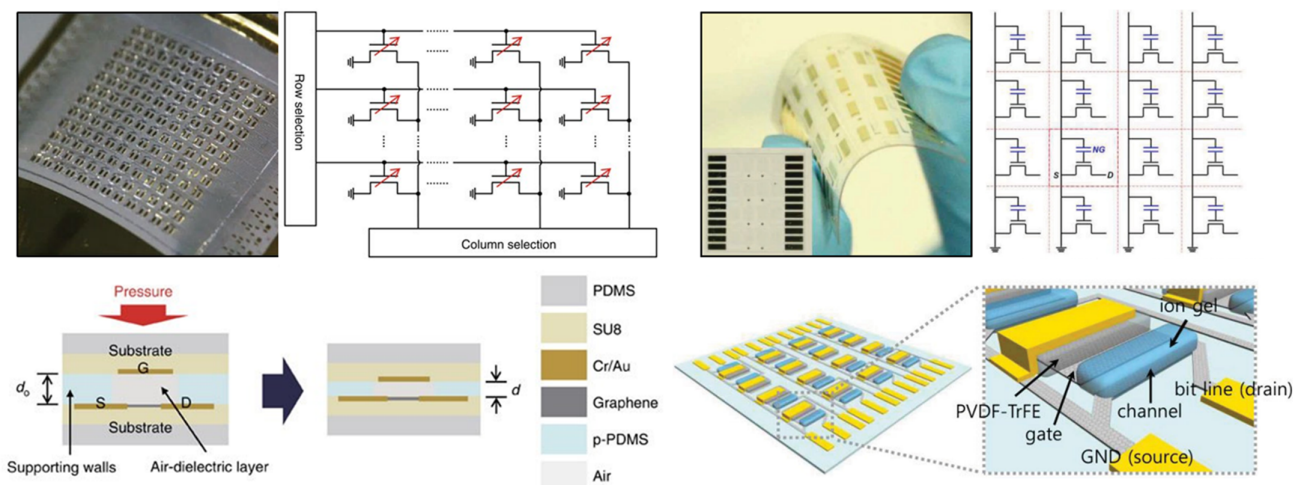
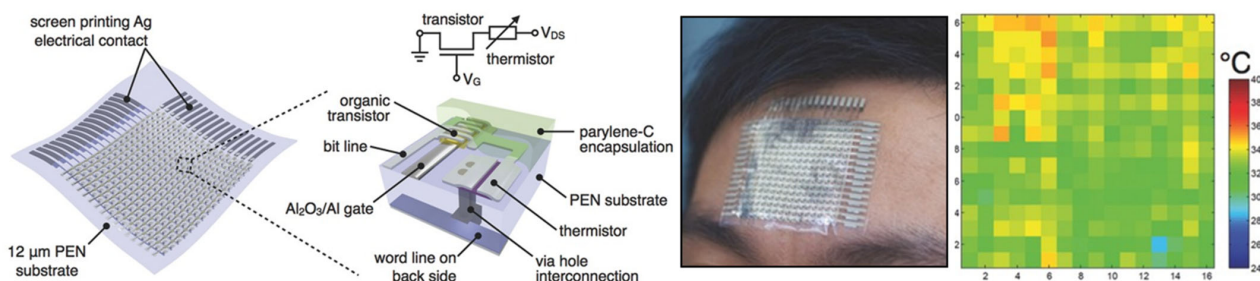


Figure 11. Graphene TFT active matrix flexible pressure and strain sensors. a) Air-dielectric graphene TFT active matrix pressure sensor. The top-gated graphene TFTs with local air gaps as the dielectrics show pressure-sensitive capacitance change, which enables the TFTs to act as tactile pressure sensors. Reproduced under the terms of the CC BY license.^[98] Copyright 2017, The Authors. Springer Nature. b) Piezopotential-powered graphene TFT active matrix strain sensor. Piezoelectric nanogenerators and coplanar-gate structured graphene TFTs are integrated to obtain the active matrix strain sensors. The external strain-induced piezopotentials can be effectively coupled to the TFT channels through the ion gel gate dielectrics, leading to charge accumulation in the channel. Adapted with permission.^[99] Copyright 2015, Wiley-VCH.

(a) OTFT active matrix driven temperature sensor array



(b) OTFT active matrix physiological temperature sensor

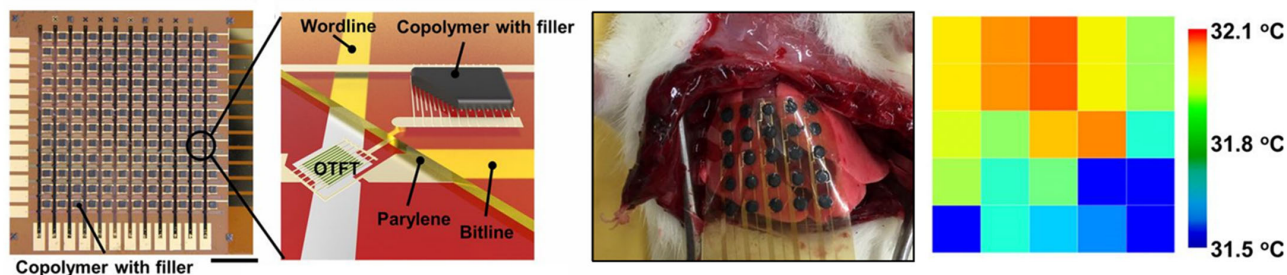


Figure 12. Active matrix flexible temperature sensors. a) OTFT active matrix temperature sensor array. The flexible temperature sensor array is constructed by integrating DNTT TFT active matrix with Ag nanoparticle/pentacene thin film thermistors. The sensor array can be used for conformal temperature measurement of the human body. Adapted with permission.^[12] Copyright 2016, Wiley-VCH Verlag GmbH & Co. KGaA. b) OTFT active matrix physiological temperature sensor. The active matrix physiological temperature sensor is fabricated by integrating DNTT TFT backplane with a highly temperature-sensitive composite. The temperature sensor exhibits high spatiotemporal resolution and a sensitivity down to 0.1 °C or less, which can be used for dynamic physiological temperature measurement in the lung during very fast artificial respiration. Adapted with permission.^[22] Copyright 2015, The Authors. Published National Academy of Sciences.

50 nm-thick n-type semiconductor 3,4,9,10-perylene-tetracarboxylic-diimide (PTCDI) are deposited through vacuum sublimation

to construct the organic photodiodes, which are further integrated with pentacene TFT active matrix to obtain the sheet

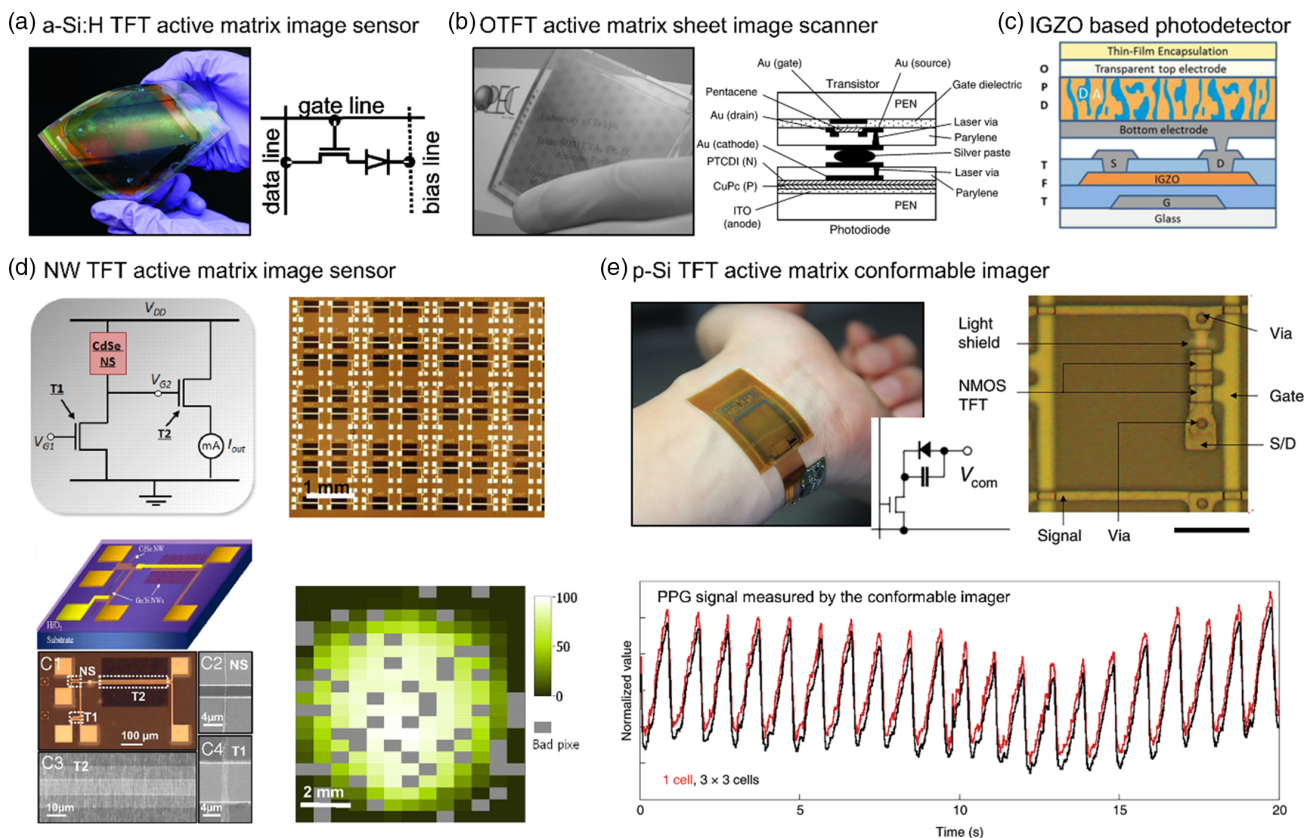


Figure 13. Active matrix flexible photodetectors. a) a-Si:H TFT active matrix image sensor. MEHPPV-PCBM bulk heterojunction organic photodiodes are integrated into a-Si:H TFT active matrix to obtain the flexible image sensor array. Adapted with permission.^[49] Copyright 2008, American Institute of Physics. b) OTFT active matrix sheet image scanner. The p-type semiconductor CuPc and n-type semiconductor PTCDI are used to construct the organic photodiodes, which are integrated with pentacene TFT active matrix for the sheet image scanner. Adapted with permission.^[69] Copyright 2005, IEEE. c) a-IGZO based photodetector. Solution-processed bulk heterojunction organic photodiodes are integrated with a-IGZO TFT active matrix to obtain the flexible photodetector. Adapted with permission.^[160] Copyright 2018, The Society for Information Display. d) Nanowire TFT active matrix image sensor. High-mobility Ge/Si nanowires are used as the TFT channel materials, and optically active CdSe nanowires are used as the photosensors for the all-integrated, heterogeneous nanowire image sensors. To increase the signal magnitude, an on-site amplification is implemented based on the nanowire circuitry. Adapted with permission.^[94] Copyright 2008, National Academy of Sciences. e) p-Si TFT active matrix conformable imager. The p-Si TFT readout circuits and near-infrared organic photodiodes are combined to create the conformable imager, which can be used for obtaining static biometric signals and dynamic PPG signals. Adapted with permission.^[24] Copyright 2020, Springer Nature Ltd.

image scanner. The effective sensing area for the scanner is $5 \times 5 \text{ cm}^2$ with a resolution of 36 dpi. The total number of the sensor pixels is 5184. The thickness of the entire device is just $400 \mu\text{m}$ with a weight of 1 g. Organic bulk heterojunction can also be printed and integrated with a-IGZO TFT active matrix for flexible scanners (Figure 13c).^[160] The scanner has an area of $6 \times 8 \text{ cm}^2$ and a resolution of 200 pixels per inch (ppi), which has been demonstrated as a palmprint scanner for biometric authentication. Image sensors based on fully integrated, all-nanowire circuitry have been reported, as shown in Figure 13d.^[94] In the heterogeneously integrated nanowire sensor system, high-mobility Ge/Si nanowires are used as the TFT channel materials, and optically active CdSe nanowires are used as the photosensors. Meanwhile, on-site amplification is implemented to increase the signal magnitude. Image sensor array with 13×20 pixels has been fabricated and used for the mapping of the projection light from a halogen light source.

Recently, p-Si TFT active matrix conformable imager has been reported (Figure 13e).^[24] The p-Si with a mobility of $40 \text{ cm}^2 \text{V}^{-1} \text{s}^{-1}$ is employed as the channel materials to realize high-resolution and fast readout. Bulk heterostructure organic photodiodes with a sensitivity in the near-infrared region is used as the photosensors. The effective sensor area for the imager is $12.6 \times 12.8 \text{ mm}^2$, with a resolution of 508 ppi. The total number of the sensor pixels is 252×256 cells, and the cell pitch is $50 \mu\text{m}$. The conformable imager is used for measuring the static biometric parameters and dynamic biosignals such as pulse waves, and it is further used to capture the entire area of photoplethysmogram (PPG) signals with a speed as high as 41 frames per second (fps). This high-definition and high-speed conformable imager will find various applications in biomedical measurements, disease diagnostics, and biometric authentication technologies.

Currently, most of the reported active matrix flexible photodetectors can only detect a specific or limited range of wavelength. Photodetector arrays with full-color detection are desired for

applications in multiple target monitoring under complex environmental conditions.^[169] Recently, quantum dot (QD)-sensitized a-IGZO hybrid phototransistor arrays have been fabricated for flexible full-color photodetectors.^[129] The a-IGZO channels are sensitized by PbS, CdS, or CdSe QDs with different diameters, allowing the QD/a-IGZO phototransistors responsive to different ranges of wavelengths from 365 to 1310 nm. The QD nanoparticles can be deposited with high spatial resolution by direct photopatterning owing to the photochemical reactivity of the $\text{Sn}_2\text{S}_6^{4-}$ ligands on their surfaces. The color discrimination is realized through photopatterning of the QDs combined with an in-pixel charge integrating circuit design. The full-color photodetector is fabricated on a 3 μm -thick PI substrate, which is capable of compliantly attaching to the human fingertip and measuring the absorption of light with different wavelengths throughout the capillary blood vessels in the finger. The full-color 2D photodetector array can realize wavelength discrimination without sophisticated interferometric optics and color filters, and is promising in bioimaging applications.

In addition to the photodetectors which are responsive to wavelengths from ultraviolet to infrared, flexible active matrix X-Ray detector arrays have also been fabricated for medical imaging and industrial inspection.^[91,115,124,170,171] Generally, the X-Ray detectors are constructed by integrating a scintillator film on top of normal photodetectors. The scintillator film converts the incident X-rays into visible photons that can be perceived by the underneath photodetectors. Various active matrix backplane and photodiode combinations have been reported for the X-Ray detectors, such as pentacene TFT active matrix with organic photodiodes,^[115] SWCNT TFT active matrix with organic photodiodes,^[91] a-IGZO TFT active matrix with amorphous silicon photodiodes,^[170] a-IGZO TFT active matrix with organic photodiodes,^[124] and a-IGZO TFT active matrix with perovskite photodiodes.^[171]

5.4. Magnetic Sensors

During the last few years, magnetosensory system has been introduced to the e-skins, equipping the recipient with a “sixth sense” for perceiving the static and dynamic magnetic fields.^[172] The magnetic e-skins can be used in proximity sensors for touchless human–machine interaction, navigation, and localization for robotics, as well as the monitoring of the human body motions for early diagnostics of dysfunctions.^[173] Active matrix magnetic sensors are desired to efficiently map magnetic fields with real-time encoding of the locations and motions of magnetic objects. Recently, imperceptible active matrix magnetic e-skin has been reported (Figure 14a).^[27] The magnetic e-skin system incorporates OTFT active matrix magnetoresistance sensors, organic shift register drivers, and signal amplifier circuits in a single platform (Figure 14b). DNTT TFTs are used to construct the multiplexers for the pixel selection, as well as the driving and signal amplifying circuits. Meanwhile, giant magnetoresistance (GMR) multilayers made of permalloy ($\text{Ni}_{81}\text{Fe}_{19}$) and Cu are deposited as the sensor elements (Figure 14c). The magnetic e-skin is capable of mapping the magnetic fields with high precision. As shown in Figure 14d, 2D magnetic field mapping is demonstrated by placing a weak ferrite permanent magnet close

to the sensor matrix. The magnetic e-skin system with active matrix sensor array and on-chip integrated peripheral circuits represents a high level of sophistication and functionalization for imperceptible electronics.

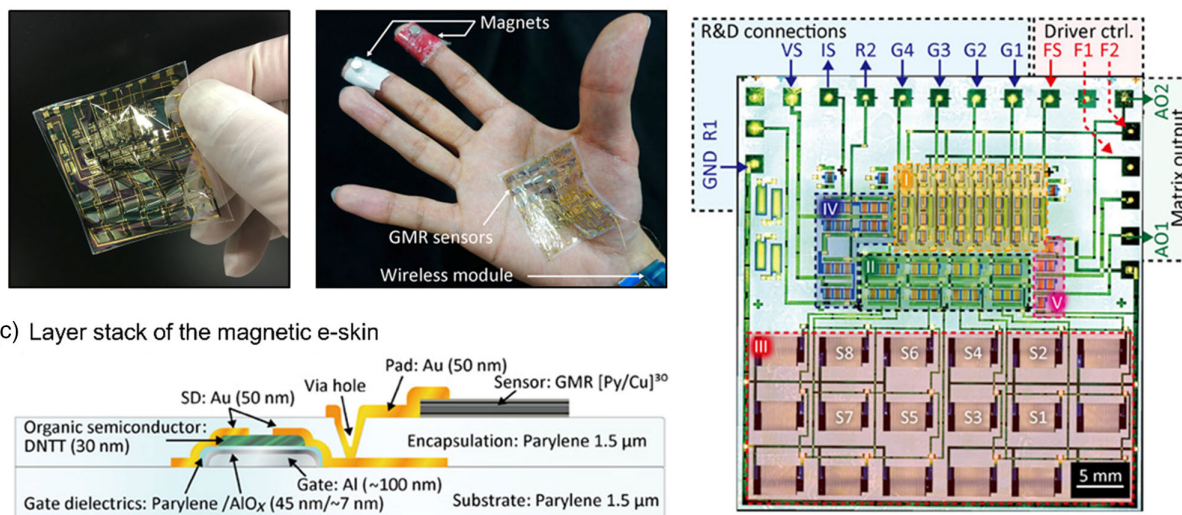
Recently, a-IGZO TFT active matrix integrated micro-origami magnetic sensor has been reported to detect the magnetic vector fields in three dimensions (Figure 15).^[23] The 3D magnetic sensor is composed of an 8×8 pixel array of self-assembled cubic architectures with biased AMR sensors fabricated by combining planar photolithography with self-folding micro-origami approach (Figure 15a). In the sensory system, a-IGZO TFTs are integrated as the active matrix backplane, and permalloy-based AMR sensors are embedded into the self-foldable polymer stacks as sensing elements. The magnetic sensor is capable of perceiving 3D magnetic fields owing to the high-density integrated pixels with three orthogonally oriented subpixels (Figure 15b). The circuit diagram of a single pixel containing three subpixels is shown in Figure 15c. In each subpixel, Wheatstone bridge configured AMR sensor is connected with a driving TFT and two readout TFTs. As discussed in the pixel design section, this special design guarantees a fast response of the matrix and a small signal crosstalk between subpixels. The 3D magnetic sensor is further integrated with a flexible composite skin layer for constructing mechanoreceptive e-skins. The composite skin is composed of a PDMS spacer and an ultraflexible Ecoflex membrane with embedded magnetic hairs. External mechanic stimuli to the artificial hairs can be detected by the underneath 3D magnetic sensor array (Figure 15d). The active matrix 3D magnetic sensory system has validated the micro-origami fabrication approach in the preparation and high-density integration of 3D sensors. The obtained 3D sensors can be used for static mapping of magnetic stray fields and dynamic tracking of magnetic objects in real time, which paves the way for their wide applications in the localization and navigation of microrobots, as well as the feedback control for robotics.

5.5. Biosignal Sensors

In addition to the broad applications in flexible and wearable electronics, the active matrix flexible sensory systems are also finding a wide spectrum of clinical and medical applications in implantable electronics.^[174] These implantable biosignal sensors are interfaced with the internal organs and tissues for the in vivo detection of electrophysiological signals such as electrocardiogram (ECG),^[26,41,71,74] electromyogram (EMG)^[72] and electrocardiogram (ECOG).^[20,42,43,73] The ultraflexibility ensures the sensors intimately adhere to the surfaces of the organs or tissues for high-fidelity signal collection meanwhile cause minimum irritation and injury. The implementation of active matrix driving technology enables the integration of a large number of distributed sensors over the surface of the organs or tissues, which can provide spatiotemporal maps of the electrophysiological signals in real time.

Figure 16 demonstrates typical active matrix flexible biosignal sensors based on silicon electronics.^[26,43,44] In these biosensors, high-quality m-Si nanomembranes are used as the TFT channel materials. The sensor devices exhibit excellent mechanical flexibility due to the usage of ultrathin substrates and proper

(a) Photographs of the imperceptible active matrix magnetic e-skin (b) Schematics of the imperceptible system



(d) Demonstration on two-dimensional mapping of magnetic field

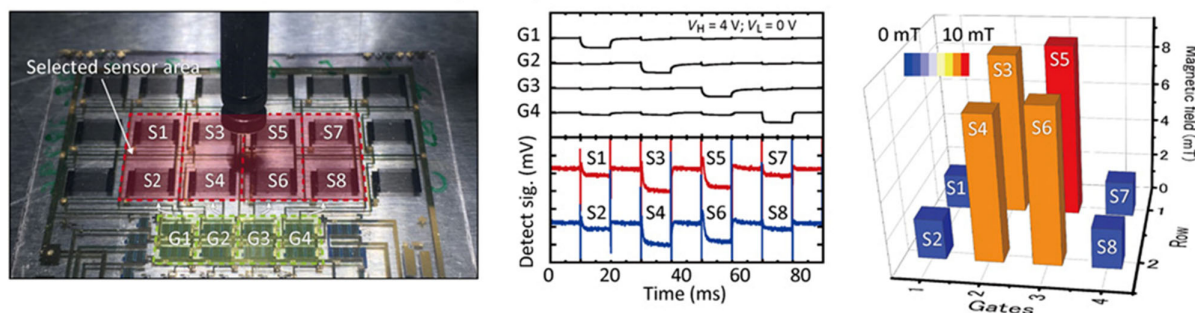


Figure 14. OTFT active matrix imperceptible magnetic e-skin. a) Photographs of the imperceptible active matrix magnetic e-skin. b) Schematics of the imperceptible system. c) Layer stack of the magnetic e-skin. d) Demonstration on 2D mapping of magnetic field. Reproduced with permission.^[27] Copyright 2020. The Authors. Published by AAAS.

encapsulation layers. The biosignal sensor with high-density active electrode array can be compliantly placed on the visual cortex for the mapping of brain activities (Figure 16a). Moreover, it can be folded around $\approx 700 \mu\text{m}$ thick silicone rubber to form a double-sided recording device. The folded device can be inserted into the medial aspects of the cerebral hemispheres or the interior of sulci that are difficult to access by other sensors.^[43]

The long-term stability of the biosensors is of vital importance for their applications in implantable electronics. Therefore, proper encapsulation and signal coupling strategies are required to prevent the penetration of biological fluids into the electronics. Figure 16b shows a capacitively coupled active matrix electrophysiological sensor.^[26] In this sensor device, the underlying electronic components are completely sealed by an ultrathin, leakage-free, and biocompatible SiO₂ dielectric layer. The electrophysiological signals are measured through capacitive coupling between the electronics and the tissue. The sensor adopts two TFTs per pixel design, with a switching TFT as the multiplexer for pixel selection and an amplifying TFT for built-in signal conditioning. The capacitively coupled biosensor exhibits excellent electrical and mechanical stabilities during the *in vitro* and *ex vivo* tests, enabling its long-term applications in

diagnostics and treatment of chronic diseases. Although the capacitively coupling strategy is useful in many application scenarios, it requires a large capacitance between the SiO₂ sensing pads and the surrounding tissue to avoid signal attenuation. In addition, the capacitive configuration is incapable of electrical stimulation. Therefore, conductively coupled active matrix neural electrophysiological sensor has been fabricated recently (Figure 16c).^[44] In this device, thermally grown SiO₂ thin film is chemically bonded to the silicon nanomembranes and employed as a leakage-free and chronically stable barrier. Au metal pads are deposited to form electrical contacts to the surrounding tissues. This configuration enables the conductively coupled sensing and electrical stimulation through Faradaic charge injection. The assessments on the electrical performance and dissolution behaviors as well as the temperature-dependent studies reveal the stability of the conductively coupled sensors, indicating their broad applications in large-area, long-lived electrical implants for electrophysiological mapping and stimulation.

The electrophysiological signals are generally weak, and sensitivity on the order of microvolts to millivolts is required for the biosensors to detect these weak signals.^[71] Therefore,

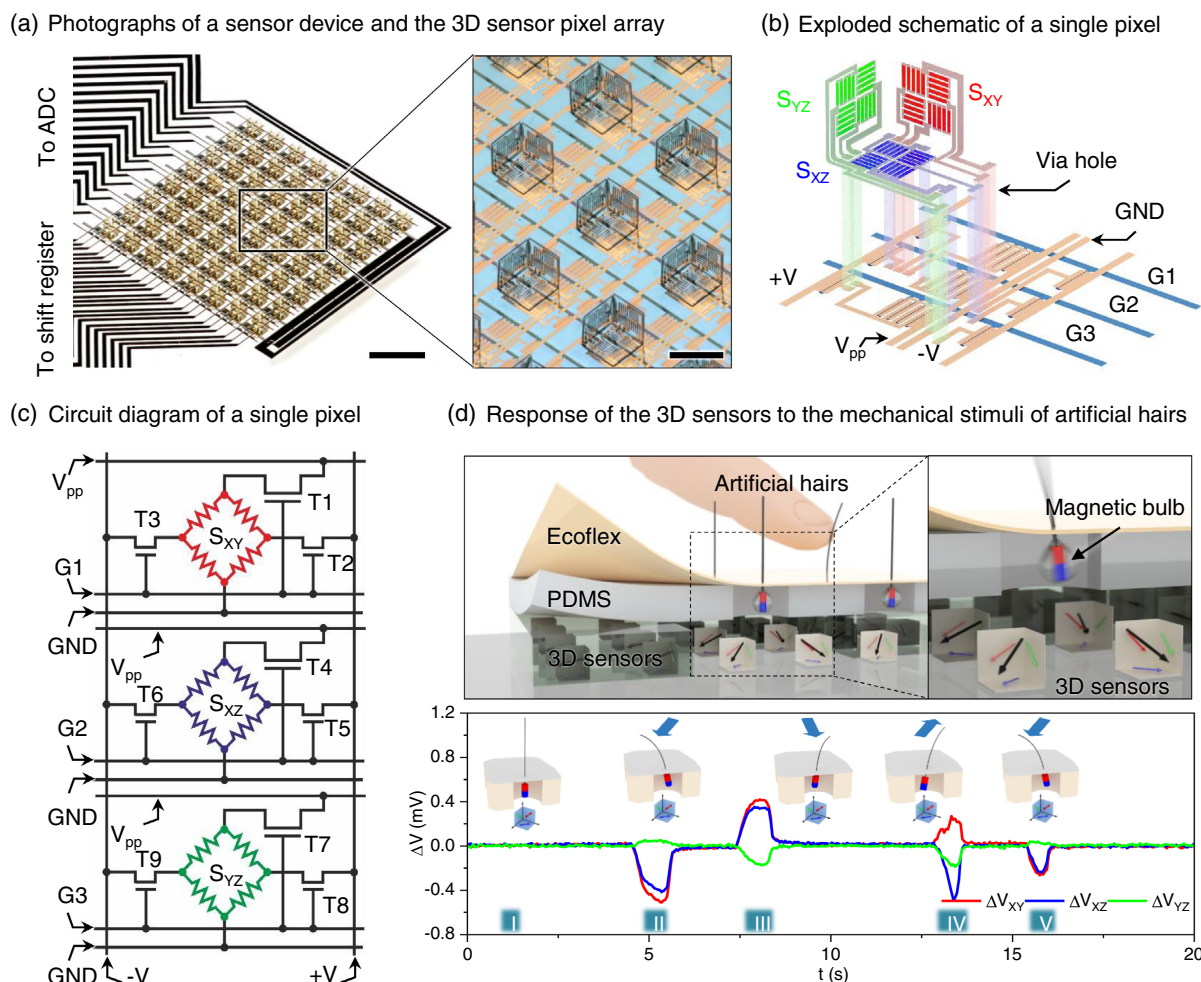


Figure 15. Active matrix integrated micro-origami sensor arrays. a) Photographs of a sensor device and the 3D sensor pixel array in the device. b) Exploded schematic showing the structure of a single pixel. c) Circuit diagram of a single pixel which contains three subpixels with Wheatstone bridge configured AMR sensors. d) Response of the 3D sensors to the mechanical stimuli of artificial hairs. Reproduced under the terms of the CC BY license.^[23] Copyright 2022, The Authors. Published by Springer Nature.

in-pixel amplification is frequently adopted to on-site condition the acquired signals. As shown in Figure 16b,c, single TFTs have been integrated as amplifiers by coupling the input signals to their gate electrodes. Recently, more complex amplifying circuits have been integrated within the pixels based on silicon and organic electronics.^[41,71] The silicon amplifiers have source-follower configuration with current gain, and are addressed by the multiplexing TFTs in the active matrix. The amplifier shows a high bandwidth with a cutoff frequency of ≈ 200 kHz owing to the high mobility ($\approx 490 \text{ cm}^2 \text{ V}^{-1} \text{ s}^{-1}$) of the m-Si TFT components. The biosensor is used for mapping cardiac electrophysiology in a porcine model. The spreads of spontaneous and paced ventricular depolarization can be mapped in real time by attaching the sensor on the epicardial surface.^[41] The organic amplifier is composed of an inverter, a capacitor, and a resistor. The inverter adopts a pseudo-CMOS layout with four DNTT TFTs. The organic amplifier matrix is combined with highly conductive multiwalled CNT composite gel electrodes for epicardial ECG monitoring. The amplifier exhibits excellent amplification

performance with a large gain. A 1.2 mV input signal is amplified to a 200 mV output signal with a gain of ≈ 200 .^[71]

Besides the silicon and organic TFT active matrix biosensors, OECT active matrix multielectrode arrays have emerged as a new kind of transducers for monitoring bioelectrical signals in recent years, owing to their large transconductance, ease of fabrication, and large flexibility in device architecture.^[78,79,117,120] The integration of OECT active matrix in biosensors enables local signal amplification and multiple pixel addressing at the same time. State-of-the-art OECTs for in vivo electrophysiological recordings are mostly based on the conducting polymer PEDOT:PSS. **Figure 17** demonstrates several applications of PEDOT:PSS OECT active matrix biosensors. For example, the PEDOT:PSS OECTs have been used in ECoG probes (Figure 17a).^[20] The total thickness of the probes is just around $4 \mu\text{m}$, making them highly conformable meanwhile strong enough for handling. The output and transfer curves demonstrate that the PEDOT:PSS OECT works in the depletion regime with a low operation voltage of 0.5 V. The direct contact with the electrolyte enables efficient

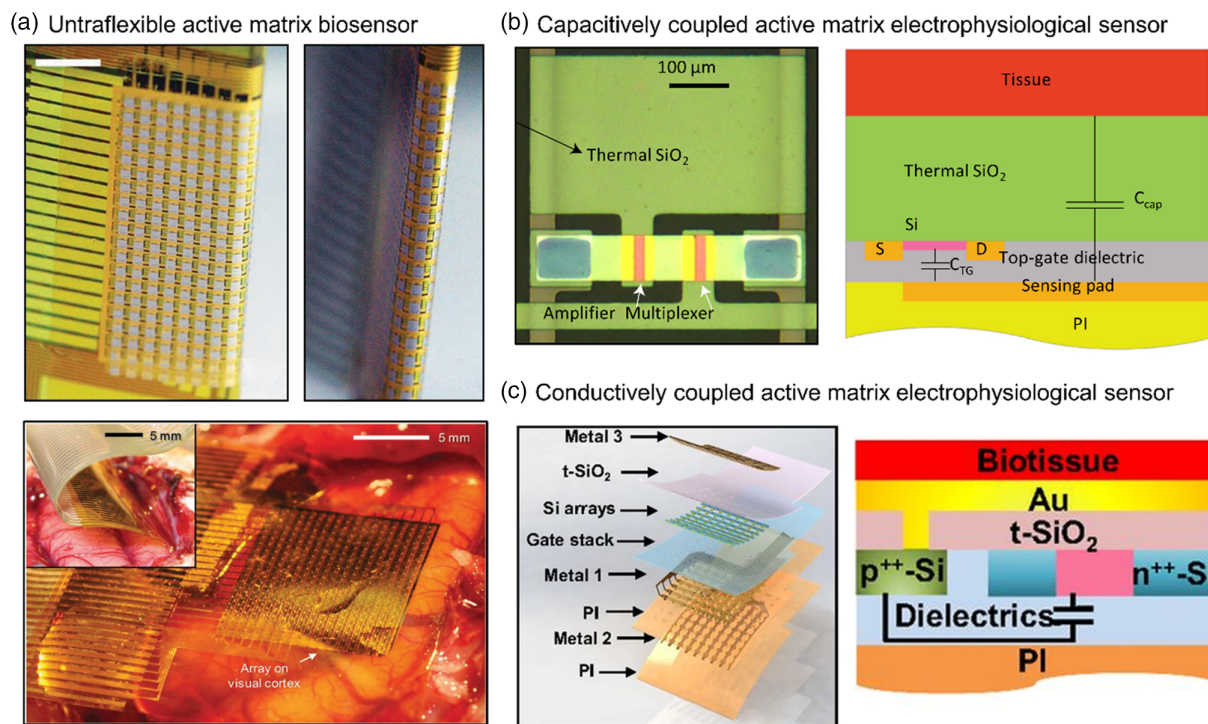


Figure 16. Active matrix flexible biosignal sensors based on silicon electronics. a) Ultraflexible active matrix biosensor. The sensor array can be folded around low modulus PDMS insert, placed on the visual cortex and inserted into the interhemispheric fissure. Adapted with permission.^[43] Copyright 2011, Nature Publishing Group. b) Capacitively coupled active matrix electrophysiological sensor. Optical microscope image, schematic of the circuit cross section and circuit diagram of a single pixel showing the mechanism of capacitively coupled sensing. Adapted with permission.^[26] Copyright 2017, Macmillan Publishers Ltd. c) Conductively coupled active matrix neural electrophysiological sensor. Exploded view of the layer stacks, schematic of the circuit cross section and circuit diagram of a single pixel showing the mechanism of conductively coupled sensing. Adapted with permission.^[44] Copyright 2018, The Authors. Published by National Academy of Sciences.

gating of the PEDOT:PSS channel. The normalized transconductance of the PEDOT:PSS OEET is several orders of magnitude higher than typical silicon and organic TFTs. The OEET is wired in a common source configuration and the grounded screw is used as gate electrode for the *in vivo* recording of the brain activities. The OEET probes can realize superior gain recording with a high signal noise ratio (SNR) owing to the local signal amplification.

Recently, transparent PEDOT:PSS OEET active matrix biosensor has been reported by integrating Au metal grid wirings as the transparent electrodes (Figure 17b).^[73] Due to the intrinsic transparency of the PEDOT:PSS channels, the entire area of the obtained device is highly transparent, which enables its applications in optogenetics. The spatial mapping of ECoG signals from an optogenetic rat exhibits high signal integrity showing lower light artifacts than the noise level. Although with high flexibility, it is still challenging to conformally interface the OEET active matrix sensors with soft and dynamically moving organs such as the surface of the heart for long-term recording. To overcome this limitation, stretchable PEDOT:PSS OEET active matrix biosensor has been fabricated (Figure 17c).^[74] In this device, honeycomb grid perylene is used as substrate to realize stretchability. Meanwhile, the surface of the device is coated by a nonthrombogenic agent poly(3-methoxypropyl acrylate) to increase the blood compatibility. The stretchable and blood compatible biosensor is used for the ECG measurement on the heart surface of rats. A

high SNR of 52 dB can be achieved owing to the conformal contact interface, the suppression of blood clots, and the high transconductance of the PEDOT:PSS OEETs. Moreover, the motion artifact noise can be efficiently suppressed because of the high compliance of the stretchable microgrid structures.

In addition to the biosensors with OEETs that function both as sensors and multiplexers, active matrix electrophysiological sensors which are integrated with OEETs as sensor elements and OTFTs as multiplexers have been reported (Figure 17d).^[72] In this biosensor, each detection cell contains one PEDOT:PSS OEET and one DNNT TFT. The cutoff frequency of the integrated device is ≈ 3 kHz and the transconductance is large than 1 mS. The total thickness of the device is 2.0 μm . It can be conformably laminated onto the surface of the optogenetic rat's gracilis muscle for EMG signal mapping with negligible mechanical interference during the motion of the muscles. Millisecond-scale myoelectric signal can be detected which involves with the muscle contraction of the optogenetic rat by blue light stimulation.

6. Conclusion and Outlook

The active matrix flexible sensory systems have seen remarkable advances and breakthroughs during the last two decades, enabling modern application scenarios such as e-skins, implantable and wearable electronics, which bridges the gap between the

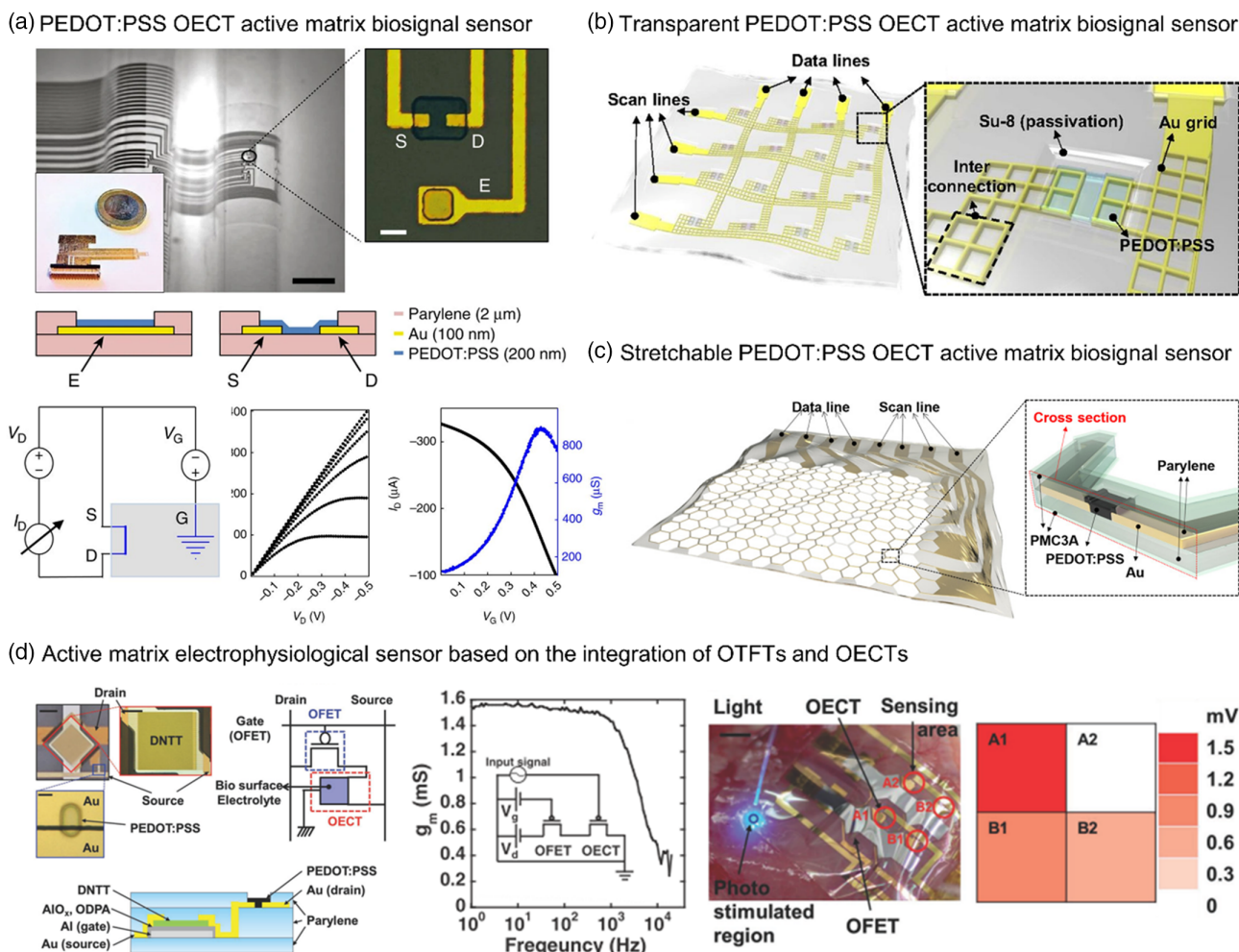


Figure 17. OECT active matrix flexible biosignal sensors. a) PEDOT:PSS OECT active matrix biosignal sensor. The optical micrographs show the whole sensor device and magnified view of a PEDOT:PSS OECT and a surface electrode. The schematic illustrations show the layouts of the surface electrode and the OECT channel. The wiring layout illustrates the operation mechanism of the OECT. The output and transfer curves show the electrical performance. Adapted with permission.^[20] Copyright 2013, Macmillan Publishers Ltd. b) Transparent PEDOT:PSS OECT active matrix biosignal sensor. Image of the OECT active matrix on a parylene substrate and magnified image of a single pixel are demonstrated. Adapted with permission.^[73] Copyright 2017, National Academy of Sciences. c) Stretchable PEDOT:PSS OECT active matrix biosignal sensor. Image of the OECT active matrix on a honeycomb grid parylene substrate and cross section of the OECT are shown. Adapted with permission.^[74] Copyright 2018, The Authors. Published by AAAS. d) Active matrix electrophysiological sensor based on the integration of OTFTs and OECTs. Detailed front view, schematic circuit diagram, and illustration of the cross section for a single pixel are shown. The transconductance of the device is responsive to the frequency of the input signal with a cutoff frequency of ≈ 3 kHz. The sensor is attached on the muscle tissue of optogenetic mice with continuous stimulation by a blue laser for the measurement of myoelectric signal intensity. Adapted with permission.^[72] Copyright 2016, Wiley-VCH Verlag GmbH & Co. KGaA.

natural and artificial systems. The usage of ultrathin substrates, adoption of neutral mechanical plain designs, and application of high-performance thin-film materials have dramatically impacted the form factor of the sensory systems. This leads to an evolution of the form factor from flexible to ultraflexible, foldable, crumplable, stretchable, and implantable. The envisioned goal for these new forms of flexible sensory systems is to provide compliant and high spatial resolution perceptual capabilities for the humans and robotic appliances, improving their interactions with the external environment.

Flexible TFTs, as the enabling component for the active matrix sensory systems, have been significantly improved over the last two decades. The channel materials for the TFT active matrices

are represented with a large number of semiconductors, including conventional silicon in different crystalline forms, organic and oxide semiconductors, 1D nanotubes and nanowires, as well as the recently emerging 2D semiconductors. The implementations of high-quality organic/inorganic hybrid dielectric and ionic dielectric materials have significantly lowered the device operation voltage down to several voltages or less, allowing the wearable electronics to be power efficient and the implantable electronics to safely work in aqueous environments. The pixels in the active matrix flexible sensory systems have evolved from simple circuits with one TFT and one sensing element configuration to advanced designs with numerous transistors, realizing in-pixel integrated amplifiers for local signal conditioning.

Moreover, light-emitting and nonvolatile memory devices have been respectively integrated into the pixels for the visualization and storage of the detected information. The fabrication technologies for the flexible sensory systems have evolved from conventional photolithography and shadow mask-assisted deposition to solution-based processing and large-area printing. The direct ink printing techniques have shown enormous potential and will be among the mainstream technologies to decrease the device fabrication price and bring the active matrix flexible sensors to large-scale practical applications. All these developments have greatly prompted the advancement of the active matrix flexible sensory systems, facilitating their wide range of applications in the detection of signals including tactile pressure, temperature, light, magnetic field, and electrophysiological activities, to name a few.

Despite the rapid progress that has been made in the active matrix flexible sensory systems, numerous opportunities and challenges are still remaining requiring further research and development. Among these challenges, improvement of the yield and performance of the flexible TFTs, design of unipolar circuits as well as the compatibility with sensory technologies are the crucial points that have to be solved for the realization of fully integrated active matrix flexible sensory systems in a monolithic technological process. So far, most of the active matrix flexible sensors can only have response to one kind of stimulus which limits their applications, for instance, in e-skins. There are just a very few reports on the bifunctional active matrix flexible sensors, achieved either by overlapping two active matrix sensor arrays^[29] or by employing special nanocomposite transducers with dual responses.^[52,175] The human skin is a complex system embedded with different types of highly specialized sensory receptors to convert various environment stimuli into the electrical impulses.^[176] To fabricate artificial e-skin systems with augmented capabilities compared to their nature counterparts, heterogeneous integration of multiple sensing modalities within one active matrix array is highly desired (Figure 1 and 3).^[86] For example, dissimilar sensing elements could be integrated into different pixels in the same active matrix array, creating a heterogenous active matrix flexible sensory system with responses to multiple stimuli.^[177] Besides the detection of physical and electrophysiological signals, the detection of chemical biomarkers from the breath, sweat, saliva, and other secretions in the active matrix format could be an opportunity for the flexible sensory systems, which can provide means for batch chemical analysis to obtain spatiotemporal patterns of the biomarkers.^[178–180] For example, active matrix flexible biochemical sensors could be used for continuously monitoring the pH values distributed across the wound during healing process.^[181] The blending of wearable chemical sensors with the active matrix addressing technology would have tremendous potential in digital health and personalized medicine. From the fabrication point of view, it is quite challenging to obtain devices with such high level of sophistication. Therefore, different fabrication strategies should be combined together to simplify the integration workflow. For instance, the active matrix backplanes can be fabricated by photolithography and the diverse transducing elements can be additive obtained by inkjet printing.

Improvement of the circuit design could lead to decrease of interconnect numbers and increase of the freedom in the final application design. Therefore, some peripheral circuits such as

the row and column drivers could also be integrated into the flexible sensory systems.^[27,182,183] The challenge lies within the successful integration of these driver circuits in large area with high yield. Therefore, new advanced circuit designs and fabrication strategies are expected in the near future. Active matrix flexible sensory systems with on-board energy source and wireless data transmission are expected in a long-term goal. Such heterogeneously integrated active matrix flexible sensory systems would find numerous applications in robotics, human-machine interfaces, medical diagnostics, and prosthetic devices. This research topic is highly multidisciplinary, and future joint efforts from chemist, materials scientists, electronic engineers, and biologists are expected to develop new material systems, promote novel sensory mechanisms, realize higher level of function integrations, and explore a broader range of applications for the sensory systems.

Acknowledgements

This work was supported by the German Research Foundation DFG (Gottfried Wilhelm Leibniz Prize granted in 2018, SCHM 1298/22-1, KA5051/1-1, and KA5051/3-1). This work was also supported by the Leibniz Association (T62/2019). Y.S. thanks the support of the National Key R&D Program of China (grant no. 2018YFA0208501), the NSFC (grant nos. 91963212 and 51961145102), and Beijing National Laboratory for Molecular Sciences (grant no. BNLMS-CXXM-202005).

Open Access funding enabled and organized by Projekt DEAL.

Conflict of Interest

The authors declare no conflict of interest.

Keywords

active matrices, electronic skins (e-skins), flexible electronics, flexible sensors, heterogeneous integration, inkjet printing, thin-film transistors

Received: December 6, 2021

Revised: April 3, 2022

Published online:

- [1] S.-T. Han, H. Peng, Q. Sun, S. Venkatesh, K.-S. Chung, S. C. Lau, Y. Zhou, V. A. L. Roy, *Adv. Mater.* **2017**, 29, 1700375.
- [2] S. Yuvaraja, A. Nawaz, Q. Liu, D. Dubal, S. G. Surya, K. N. Salama, P. Sonar, *Chem. Soc. Rev.* **2020**, 49, 3423.
- [3] Y. H. Lee, M. Jang, M. Y. Lee, O. Y. Kweon, J. H. Oh, *Chem.* **2017**, 3, 724.
- [4] A. Chortos, J. Liu, Z. Bao, *Nat. Mater.* **2016**, 15, 937.
- [5] Y. Zang, F. Zhang, C. Di, D. Zhu, *Mater. Horiz.* **2015**, 2, 140.
- [6] H. Wang, X. Ma, Y. Hao, *Adv. Mater. Interfaces* **2017**, 4, 1600709.
- [7] Q. Hua, J. Sun, H. Liu, R. Bao, R. Yu, J. Zhai, C. Pan, Z. L. Wang, *Nat. Commun.* **2018**, 9, 244.
- [8] B. Shih, D. Shah, J. Li, T. G. Thuruthel, Y.-L. Park, F. Lida, Z. Bao, R. Kramer-Bottiglio, M. T. Tolley, *Sci. Rob.* **2020**, 5, eaaz9239.
- [9] E. I. Haskal, M. Büchel, P. C. Duineveld, A. Sempel, P. van de Weijer, *MRS Bull.* **2002**, 27, 864.
- [10] Y. Chen, J. Au, P. Kazlas, A. Ritenour, H. Gates, M. McCreary, *Nature* **2003**, 423, 136.

- [11] A. E. Aliev, H. W. Shin, *Displays* **2002**, *23*, 239.
- [12] X. Ren, K. Pei, B. Peng, Z. Zhang, Z. Wang, X. Wang, P. K. L. Chan, *Adv. Mater.* **2016**, *28*, 4832.
- [13] K. Myny, *Nat. Electron.* **2018**, *1*, 30.
- [14] M.-Z. Li, S.-T. Han, Y. Zhou, *Adv. Intell. Syst.* **2020**, *2*, 2000113.
- [15] H. Shim, K. Sim, F. Ershad, S. Jang, C. Yu, *J. Mater. Chem. C* **2020**, *8*, 10719.
- [16] J. A. Rogers, Z. Bao, K. Baldwin, A. Dodabalapur, B. Crone, V. R. Raju, V. Kuck, H. Katz, K. Amundson, J. Ewing, P. Drzaic, *Proc. Natl. Acad. Sci. U. S. A.* **2001**, *98*, 4835.
- [17] T. Sekitani, U. Zschieschang, H. Klauk, T. Someya, *Nat. Mater.* **2010**, *9*, 1015.
- [18] M. Kaltenbrunner, T. Sekitani, J. Reeder, T. Yokota, K. Kuribara, T. Tokuhara, M. Drack, R. Schwödauer, I. Graz, S. Bauer-Gogonea, S. Bauer, T. Someya, *Nature* **2013**, *499*, 458.
- [19] T. Sekitani, Y. Noguchi, K. Hata, T. Fukushima, T. Aida, T. Someya, *Science* **2008**, *321*, 1468.
- [20] D. Khodagholy, T. Doublet, P. Quilichini, M. Gurfinkel, P. Leleux, A. Ghestem, E. Ismailova, T. Hervé, S. Sanaur, C. Bernard, G. G. Malliaras, *Nat. Commun.* **2013**, *4*, 1575.
- [21] C. Yeom, K. Chen, D. Kiriya, Z. Yu, G. Cho, A. Javey, *Adv. Mater.* **2015**, *27*, 1561.
- [22] T. Yokota, Y. Inoue, Y. Terakawa, J. Reeder, M. Kaltenbrunner, T. Ware, K. Yang, K. Mabuchi, T. Murakawa, M. Sekino, W. Voit, T. Sekitani, T. Someya, *Proc. Natl. Acad. Sci. U. S. A.* **2015**, *112*, 14533.
- [23] C. Becker, B. Bao, D. D. Karnaushenko, V. K. Bandari, B. Rivkin, Z. Li, M. Faghih, D. Karnaushenko, O. G. Schmidt, *Nat. Commun.* **2022**, *13*, 2121.
- [24] T. Yokota, T. Nakamura, H. Kato, M. Mochizuki, M. Tada, M. Uchida, S. Lee, M. Koizumi, W. Yukita, A. Takimoto, T. Someya, *Nat. Electron.* **2020**, *3*, 113.
- [25] M. Choi, S.-R. Bae, L. Hu, A. T. Hoang, S. Y. Kim, J.-H. Ahn, *Sci. Adv.* **2020**, *6*, eabb5898.
- [26] H. Fang, K. J. Yu, C. Gloschat, Z. Yang, E. Song, C.-H. Chiang, J. Zhao, S. M. Won, S. Xu, M. Trumpis, Y. Zhong, S. W. Han, Y. Xue, D. Xu, S. W. Choi, G. Cauwenberghs, M. Kay, Y. Huang, J. Viventi, I. R. Efimov, J. A. Rogers, *Nat. Biomed. Eng.* **2017**, *1*, 38.
- [27] M. Kondo, M. Melzer, D. Karnaushenko, T. Uemura, S. Yoshimoto, M. Akiyama, Y. Noda, T. Araki, O. G. Schmidt, T. Sekitani, *Sci. Adv.* **2020**, *6*, eaay6094.
- [28] E. K. Lee, C. H. Park, J. Lee, H. R. Lee, C. Yang, J. H. Oh, *Adv. Mater.* **2017**, *29*, 1605282.
- [29] T. Someya, Y. Kato, T. Sekitani, S. Iba, Y. Noguchi, Y. Murase, H. Kawaguchi, T. Sakurai, *Proc. Natl. Acad. Sci. U. S. A.* **2005**, *102*, 12321.
- [30] P. H. Lau, K. Takei, C. Wang, Y. Ju, J. Kim, Z. Yu, T. Takahashi, G. Cho, A. Javey, *Nano Lett.* **2013**, *13*, 3864.
- [31] K. Fukuda, Y. Takeda, Y. Yoshimura, R. Shiwaku, L. T. Tran, T. Sekine, M. Mizukami, D. Kumaki, S. Tokito, *Nat. Commun.* **2014**, *5*, 4147.
- [32] W. Lee, H. Koo, J. Sun, J. Noh, K.-S. Kwon, C. Yeom, Y. Choi, K. Chen, A. Javey, G. Cho, *Sci. Rep.* **2015**, *5*, 17707.
- [33] M. Fattori, J. Fijn, P. Harpe, M. Charbonneau, S. Lombard, K. Romanjek, D. Locatelli, L. Tournon, C. Laugier, E. Cantatore, *IEEE Electron Device Lett.* **2019**, *40*, 1682.
- [34] H. Zhang, Y. Liu, C. Yang, L. Xiang, Y. Hu, L.-M. Peng, *Adv. Mater.* **2018**, *30*, 1805408.
- [35] G. A. Salvatore, N. Münzenrieder, T. Kinkeldei, L. Petti, C. Zysset, I. Strebel, L. Büthe, G. Tröster, *Nat. Commun.* **2014**, *5*, 2982.
- [36] D. S. Wie, Y. Zhang, M. K. Kim, B. Kim, S. Park, Y.-J. Kim, P. P. Irazoqui, X. Zheng, B. Xu, C. H. Lee, *Proc. Natl. Acad. Sci. U. S. A.* **2018**, *115*, E7236.
- [37] L. Petti, N. Münzenrieder, C. Vogt, H. Faber, L. Büthe, G. Cantarella, F. Bottacchi, T. D. Anthopoulos, G. Tröster, *Appl. Phys. Rev.* **2016**, *3*, 021303.
- [38] B. Wang, A. Facchetti, *Adv. Mater.* **2019**, *31*, 1901408.
- [39] Y. Sun, J. A. Rogers, *Adv. Mater.* **2007**, *19*, 1897.
- [40] H. Sirringhaus, *Adv. Mater.* **2014**, *26*, 1319.
- [41] J. Viventi, D.-H. Kim, J. D. Moss, Y.-S. Kim, J. A. Blanco, N. Annetta, A. Hicks, J. Xiao, Y. Huang, D. J. Callans, J. A. Rogers, B. Litt, *Sci. Transl. Med.* **2010**, *2*, 24ra22.
- [42] K. J. Yu, D. Kuzum, S.-W. Hwang, B. H. Kim, H. Juul, N. H. Kim, S. M. Won, K. Chiang, M. Trumpis, A. G. Richardson, H. Cheng, H. Fang, M. Thompson, H. Bink, D. Talos, K. J. Seo, H. N. Lee, S.-K. Kang, J.-H. Kim, J. Y. Lee, Y. Huang, F. E. Jensen, M. A. Dichter, T. H. Lucas, J. Viventi, B. Litt, J. A. Rogers, *Nat. Mater.* **2016**, *15*, 782.
- [43] J. Viventi, D.-H. Kim, L. Vigeland, E. S. Frechette, J. A. Blanco, Y.-S. Kim, A. E. Avrin, V. R. Tiruvadi, S.-W. Hwang, A. C. Vanleer, D. F. Wulsin, K. Davis, C. E. Gelber, L. Palmer, J. Van der Spiegel, J. Wu, J. Xiao, Y. Huang, D. Contreras, J. A. Rogers, B. Litt, *Nat. Neurosci.* **2011**, *14*, 1599.
- [44] J. Li, E. Song, C.-H. Chiang, K. J. Yu, J. Koo, H. Du, Y. Zhong, M. Hill, C. Wang, J. Zhang, Y. Chen, L. Tian, Y. Zhong, G. Fang, J. Viventi, J. A. Rogers, *Proc. Natl. Acad. Sci. U. S. A.* **2018**, *115*, E9542.
- [45] M. Park, M.-S. Kim, Y.-K. Park, J.-H. Ahn, *Appl. Phys. Lett.* **2015**, *106*, 43502.
- [46] J. Jang, B. Oh, S. Jo, S. Park, H. S. An, S. Lee, W. H. Cheong, S. Yoo, J.-U. Park, *Adv. Mater. Technol.* **2019**, *4*, 1900082.
- [47] Z. W. Yang, Y. Pang, L. Zhang, C. Lu, J. Chen, T. Zhou, C. Zhang, Z. L. Wang, *ACS Nano* **2016**, *10*, 10912.
- [48] G. Fortunato, L. Maiolo, F. Maita, A. Minotti, S. Mirabella, V. Strano, G. Metta, D. Ricci, A. Pecora, in *21st Int. Workshop on Active-Matrix Flatpanel Displays and Devices*, **2014**, pp. 311–314.
- [49] T. N. Ng, W. S. Wong, M. L. Chabiny, S. Sambandan, R. A. Street, *Appl. Phys. Lett.* **2008**, *92*, 213303.
- [50] T. N. Ng, W. S. Wong, R. A. Lujan, B. Russo, M. L. Chabiny, S. Sambandan, R. A. Street, in *Proc. SPIE*, **2008**.
- [51] H. Gleskova, S. Wagner, *IEEE Electron Device Lett.* **1999**, *20*, 473.
- [52] I. Graz, M. Krause, S. Bauer-Gogonea, S. Bauer, S. P. Lacour, B. Ploss, M. Zirkel, B. Stadlober, S. Wagner, *J. Appl. Phys.* **2009**, *106*, 34503.
- [53] S. H. Won, J. Ryu II, J. H. Hur, J. Jang, G. J. Jang, C. W. Lee, S. T. Jung, *SID Symp. Dig. Tech. Pap.* **2001**, *32*, 52.
- [54] J. T. Smith, E. Bawolek, J. Trujillo, G. Raupp, D. R. Allee, J. B. Christen, in *IEEE Int. Symp. on Circuits and Systems*, IEEE, Piscataway, NJ **2017**, pp. 1–4.
- [55] S. Hava, M. Auslender, in (Eds: S. Kasap, P. Capper), Springer US, Boston, MA, **2007**, pp. 441–480.
- [56] M. A. Meitl, Z.-T. Zhu, V. Kumar, K. J. Lee, X. Feng, Y. Y. Huang, I. Adesida, R. G. Nuzzo, J. A. Rogers, *Nat. Mater.* **2006**, *5*, 33.
- [57] H. Gleskova, P. I. Hsu, Z. Xi, J. C. Sturm, Z. Suo, S. Wagner, *J. Non. Cryst. Solids* **2004**, *338–340*, 732.
- [58] H. Dong, X. Fu, J. Liu, Z. Wang, W. Hu, *Adv. Mater.* **2013**, *25*, 6158.
- [59] C. Wang, H. Dong, W. Hu, Y. Liu, D. Zhu, *Chem. Rev.* **2012**, *112*, 2208.
- [60] Y. Wang, L. Sun, C. Wang, F. Yang, X. Ren, X. Zhang, H. Dong, W. Hu, *Chem. Soc. Rev.* **2019**, *48*, 1492.
- [61] C. Wang, H. Dong, L. Jiang, W. Hu, *Chem. Soc. Rev.* **2018**, *47*, 422.
- [62] T. Someya, T. Sekitani, *Procedia Chem.* **2009**, *1*, 9.
- [63] J. Sun, H. Park, Y. Jung, G. Rajbhandari, B. B. Maskey, A. Sapkota, Y. Azuma, Y. Majima, G. Cho, *ACS Omega* **2017**, *2*, 5766.
- [64] T. Someya, T. Sekitani, S. Iba, Y. Kato, H. Kawaguchi, T. Sakurai, *Proc. Natl. Acad. Sci. U. S. A.* **2004**, *101*, 9966.
- [65] T. Sekitani, T. Yokota, U. Zschieschang, H. Klauk, S. Bauer, K. Takeuchi, M. Takamiya, T. Sakurai, T. Someya, *Science* **2009**, *326*, 1516.

- [66] S. Lee, A. Reuveny, J. Reeder, S. Lee, H. Jin, Q. Liu, T. Yokota, T. Sekitani, T. Isoyama, Y. Abe, Z. Suo, T. Someya, *Nat. Nanotechnol.* **2016**, *11*, 472.
- [67] Y. Noguchi, T. Sekitani, T. Someya, *Appl. Phys. Lett.* **2006**, *89*, 253507.
- [68] S. Nishi, T. Miyoshi, H. Endoh, T. Kamata, *NIP Digital Fabrication Conf.* **2016**, p. 305.
- [69] T. Someya, Y. Kato, S. Iba, Y. Noguchi, T. Sekitani, H. Kawaguchi, T. Sakurai, *IEEE Trans. Electron Devices* **2005**, *52*, 2502.
- [70] X. Hou, W. Tang, S. Chen, J. Liang, H. Xu, B. Ouyang, M. Li, Y. Song, C.-C. Chen, P. Too, X. Wei, L. Jin, G. Qi, X. Guo, in *5th IEEE Electron Devices Technology & Manufacturing Conf.*, IEEE, Piscataway, NJ **2021**, pp. 1–3.
- [71] T. Sekitani, T. Yokota, K. Kuribara, M. Kaltenbrunner, T. Fukushima, Y. Inoue, M. Sekino, T. Isoyama, Y. Abe, H. Onodera, T. Someya, *Nat. Commun.* **2016**, *7*, 11425.
- [72] W. Lee, D. Kim, J. Rivnay, N. Matsuhisa, T. Lonjaret, T. Yokota, H. Yawo, M. Sekino, G. G. Malliaras, T. Someya, *Adv. Mater.* **2016**, *28*, 9722.
- [73] W. Lee, D. Kim, N. Matsuhisa, M. Nagase, M. Sekino, G. G. Malliaras, T. Yokota, T. Someya, *Proc. Natl. Acad. Sci. U. S. A.* **2017**, *114*, 10554.
- [74] W. Lee, S. Kobayashi, M. Nagase, Y. Jimbo, I. Saito, Y. Inoue, T. Yambe, M. Sekino, G. G. Malliaras, T. Yokota, M. Tanaka, T. Someya, *Sci. Adv.* **2018**, *4*, eaau2426.
- [75] Y. Chen, W. Deng, X. Zhang, M. Wang, J. Jie, *J. Phys. D. Appl. Phys.* **2021**, *55*, 53001.
- [76] K. Fukuda, K. Yu, T. Someya, *Adv. Energy Mater.* **2020**, *10*, 2000765.
- [77] G. A. Snook, P. Kao, A. S. Best, *J. Power Sources* **2011**, *196*, 1.
- [78] J. Rivnay, S. Inal, A. Salleo, R. M. Owens, M. Berggren, G. G. Malliaras, *Nat. Rev. Mater.* **2018**, *3*, 17086.
- [79] A. Nawaz, Q. Liu, W. L. Leong, K. E. Fairfull-Smith, P. Sonar, *Adv. Mater.* **2021**, *33*, 2101874.
- [80] S. Wang, J. Xu, W. Wang, G.-J. N. Wang, R. Rastak, F. Molina-Lopez, J. W. Chung, S. Niu, V. R. Feig, J. Lopez, T. Lei, S.-K. Kwon, Y. Kim, A. M. Foudeh, A. Ehrlich, A. Gasperini, Y. Yun, B. Murmann, J. B.-H. Tok, Z. Bao, *Nature* **2018**, *555*, 83.
- [81] K. Sim, Z. Rao, H.-J. Kim, A. Thukral, H. Shim, C. Yu, *Sci. Adv.* **2019**, *5*, eaav5749.
- [82] J. Y. Oh, D. Son, T. Katsumata, Y. Lee, Y. Kim, J. Lopez, H.-C. Wu, J. Kang, J. Park, X. Gu, J. Mun, N. G.-J. Wang, Y. Yin, W. Cai, Y. Yun, J. B.-H. Tok, Z. Bao, *Sci. Adv.* **2019**, *5*, eaav3097.
- [83] T. Sekitani, T. Someya, *MRS Bull.* **2012**, *37*, 236.
- [84] K. Nomura, H. Ohta, A. Takagi, T. Kamiya, M. Hirano, H. Hosono, *Nature* **2004**, *432*, 488.
- [85] Y. H. Kim, J. S. Heo, T. H. Kim, S. Park, M. H. Yoon, J. Kim, M. S. Oh, G. R. Yi, Y. Y. Noh, S. K. Park, *Nature* **2012**, *489*, 128.
- [86] B. Bao, B. Rivkin, F. Akbar, D. D. Karnaushenko, V. K. Bandari, L. Teuerle, C. Becker, S. Baunack, D. Karnaushenko, O. G. Schmidt, *Adv. Mater.* **2021**, *33*, 2101272.
- [87] J. K. Jeong, H. Won Yang, J. H. Jeong, Y. G. Mo, H. D. Kim, *Appl. Phys. Lett.* **2008**, *93*, 8.
- [88] K. Chen, W. Gao, S. Emaminejad, D. Kiriya, H. Ota, H. Y. Y. Nyein, K. Takei, A. Javey, *Adv. Mater.* **2016**, *28*, 4397.
- [89] C. Wang, D. Hwang, Z. Yu, K. Takei, J. Park, T. Chen, B. Ma, A. Javey, *Nat. Mater.* **2013**, *12*, 899.
- [90] L. Nela, J. Tang, Q. Cao, G. Tulevski, S.-J. Han, *Nano Lett.* **2018**, *18*, 2054.
- [91] T. Takahashi, Z. Yu, K. Chen, D. Kiriya, C. Wang, K. Takei, H. Shiraki, T. Chen, B. Ma, A. Javey, *Nano Lett.* **2013**, *13*, 5425.
- [92] H. Zhang, B. Wu, W. Hu, Y. Liu, *Chem. Soc. Rev.* **2011**, *40*, 1324.
- [93] M. S. Arnold, A. A. Green, J. F. Hulvat, S. I. Stupp, M. C. Hersam, *Nat. Nanotechnol.* **2006**, *1*, 60.
- [94] Z. Fan, J. C. Ho, Z. A. Jacobson, H. Razavi, A. Javey, *Proc. Natl. Acad. Sci. U. S. A.* **2008**, *105*, 11066.
- [95] K. Takei, T. Takahashi, J. C. Ho, H. Ko, A. G. Gillies, P. W. Leu, R. S. Fearing, A. Javey, *Nat. Mater.* **2010**, *9*, 821.
- [96] S. J. Kim, K. Choi, B. Lee, Y. Kim, B. H. Hong, *Annu. Rev. Mater. Res.* **2015**, *45*, 63.
- [97] Q. Sun, D. H. Kim, S. S. Park, N. Y. Lee, Y. Zhang, J. H. Lee, K. Cho, J. H. Cho, *Adv. Mater.* **2014**, *26*, 4735.
- [98] S.-H. Shin, S. Ji, S. Choi, K.-H. Pyo, B. Wan An, J. Park, J. Kim, J.-Y. Kim, K.-S. Lee, S.-Y. Kwon, J. Heo, B.-G. Park, J.-U. Park, *Nat. Commun.* **2017**, *8*, 14950.
- [99] Q. Sun, W. Seung, B. J. Kim, S. Seo, S.-W. Kim, J. H. Cho, *Adv. Mater.* **2015**, *27*, 3411.
- [100] Y. J. Park, B. K. Sharma, S. M. Shinde, M.-S. Kim, B. Jang, J.-H. Kim, J.-H. Ahn, *ACS Nano* **2019**, *13*, 3023.
- [101] J. Zhao, N. Li, H. Yu, Z. Wei, M. Liao, P. Chen, S. Wang, D. Shi, Q. Sun, G. Zhang, *Adv. Mater.* **2017**, *29*, 1702076.
- [102] F. Schwierz, *Nat. Nanotechnol.* **2010**, *5*, 487.
- [103] B. Radisavljevic, A. Radenovic, J. Brivio, V. Giacometti, A. Kis, *Nat. Nanotechnol.* **2011**, *6*, 147.
- [104] M. Choi, Y. J. Park, B. K. Sharma, S.-R. Bae, S. Y. Kim, J.-H. Ahn, *Sci. Adv.* **2018**, *4*, eaas8721.
- [105] Y. Fan, L. Li, G. Yu, D. Geng, X. Zhang, W. Hu, *Adv. Mater.* **2021**, *33*, 2003956.
- [106] C. Kim, M.-A. Yoon, B. Jang, H.-D. Kim, J.-H. Kim, A. T. Hoang, J.-H. Ahn, H.-J. Jung, H.-J. Lee, K.-S. Kim, *NPG Asia Mater.* **2021**, *13*, 44.
- [107] B. Wang, W. Huang, L. Chi, M. Al-Hashimi, T. J. Marks, A. Facchetti, *Chem. Rev.* **2018**, *118*, 5690.
- [108] M. Kimura, T. Nakanishi, K. Nomura, T. Kamiya, H. Hosono, *Appl. Phys. Lett.* **2008**, *92*, 1.
- [109] H. Dong, L. Jiang, W. Hu, *Phys. Chem. Chem. Phys.* **2012**, *14*, 14165.
- [110] R. P. Ortiz, A. Facchetti, T. J. Marks, *Chem. Rev.* **2010**, *110*, 205.
- [111] Y. Xuan, Y. Lu, S. Honda, T. Arie, S. Akita, K. Takei, *Adv. Mater. Technol.* **2021**, *6*, 2100259.
- [112] T. Takahashi, K. Takei, A. G. Gillies, R. S. Fearing, A. Javey, *Nano Lett.* **2011**, *11*, 5408.
- [113] J. Li, W. Tang, Q. Wang, W. Sun, Q. Zhang, X. Guo, X. Wang, F. Yan, *Mater. Sci. Eng. R Rep.* **2018**, *127*, 1.
- [114] W. Zhao, J. Jie, Q. Wei, Z. Lu, R. Jia, W. Deng, X. Zhang, X. Zhang, *Adv. Funct. Mater.* **2019**, *29*, 1902494.
- [115] G. H. Gelinck, A. Kumar, D. Moet, J.-L. van der Steen, U. Shafique, P. E. Malinowski, K. Myny, B. P. Rand, M. Simon, W. Rütten, A. Douglas, J. Jorritsma, P. Heremans, R. Andriessen, *Org. Electron.* **2013**, *14*, 2602.
- [116] S. H. Kim, K. Hong, W. Xie, K. H. Lee, S. Zhang, T. P. Lodge, C. D. Frisbie, *Adv. Mater.* **2013**, *25*, 1822.
- [117] F. Torricelli, D. Z. Adrahtas, Z. Bao, M. Berggren, F. Biscarini, A. Bonfiglio, C. A. Bortolotti, C. D. Frisbie, E. Macchia, G. G. Malliaras, I. McCulloch, M. Moser, T.-Q. Nguyen, R. M. Owens, A. Salleo, A. Spanu, L. Torsi, *Nat. Rev. Methods Primers* **2021**, *1*, 66.
- [118] S. Z. Bisri, S. Shimizu, M. Nakano, Y. Iwasa, *Adv. Mater.* **2017**, *29*, 1607054.
- [119] C. Sun, X. Wang, M. A. Auwalu, S. Cheng, W. Hu, *EcoMat* **2021**, *3*, e12094.
- [120] W. Lee, T. Someya, *Chem. Mater.* **2019**, *31*, 6347.
- [121] X. Wang, Z. Liu, T. Zhang, *Small* **2017**, *13*, 1602790.
- [122] D. Wang, Y. Zhang, X. Lu, Z. Ma, C. Xie, Z. Zheng, *Chem. Soc. Rev.* **2018**, *47*, 4611.
- [123] Y. S. Rim, S.-H. Bae, H. Chen, N. De Marco, Y. Yang, *Adv. Mater.* **2016**, *28*, 4415.
- [124] G. H. Gelinck, A. Kumar, D. Moet, J.-L. P. J. van der Steen, A. J. J. M. van Breemen, S. Shanmugam, A. Langen, J. Gilot, P. Groen, R. Andriessen, M. Simon, W. Ruetten, A. U. Douglas,

- R. Raaijmakers, P. E. Malinowski, K. Myny, *IEEE Trans. Electron Devices* **2016**, *63*, 197.
- [125] N. Matsuhisa, M. Kaltenbrunner, T. Yokota, H. Jinno, K. Kuribara, T. Sekitani, T. Someya, *Nat. Commun.* **2015**, *6*, 7461.
- [126] C. W. Park, J. B. Koo, C.-S. Hwang, H. Park, S. G. Im, S.-Y. Lee, *Appl. Phys. Express* **2018**, *11*, 126501.
- [127] P. Heremans, A. K. Tripathi, A. de Jamblinne de Meux, E. C. P. Smits, B. Hou, G. Pourtois, G. H. Gelinck, *Adv. Mater.* **2016**, *28*, 4266.
- [128] A. Miyamoto, S. Lee, N. F. Cooray, S. Lee, M. Mori, N. Matsuhisa, H. Jin, L. Yoda, T. Yokota, A. Itoh, M. Sekino, H. Kawasaki, T. Ebihara, M. Amagai, T. Someya, *Nat. Nanotechnol.* **2017**, *12*, 907.
- [129] J. Kim, S.-M. Kwon, Y. K. Kang, Y.-H. Kim, M.-J. Lee, K. Han, A. Facchetti, M.-G. Kim, S. K. Park, *Sci. Adv.* **2019**, *5*, eaax8801.
- [130] D. E. Mentley, *Proc. IEEE* **2002**, *90*, 453.
- [131] J. S. Chang, A. F. Facchetti, R. Reuss, *IEEE J. Emerg. Sel. Top. Circuits Syst.* **2017**, *7*, 7.
- [132] O. Vazquez-Mena, L. Gross, S. Xie, L. G. Villanueva, J. Brugger, *Microelectron. Eng.* **2015**, *132*, 236.
- [133] K. Du, J. Ding, Y. Liu, I. Wathuthanthri, C.-H. Choi, *Micromachines* **2017**, *8*, 131.
- [134] L. Jiang, H. Dong, W. Hu, *J. Mater. Chem.* **2010**, *20*, 4994.
- [135] T. Yokota, T. Sekitani, T. Tokuhara, N. Take, U. Zschieschang, H. Klauk, K. Takimiya, T. Huang, M. Takamiya, T. Sakurai, T. Someya, *IEEE Trans. Electron Devices* **2012**, *59*, 3434.
- [136] H. Fuketa, K. Yoshioka, Y. Shinozuka, K. Ishida, T. Yokota, N. Matsuhisa, Y. Inoue, M. Sekino, T. Sekitani, M. Takamiya, T. Someya, T. Sakurai, *IEEE Trans. Biomed. Circuits Syst.* **2014**, *8*, 824.
- [137] Y. Khan, A. Thielens, S. Muin, J. Ting, C. Baumbauer, A. C. Arias, *Adv. Mater.* **2020**, *32*, 1905279.
- [138] M. Su, Y. Song, *Chem. Rev.* **2021**, *122*, 5144.
- [139] M. Gao, L. Li, Y. Song, *J. Mater. Chem. C* **2017**, *5*, 2971.
- [140] W. Deng, X. Zhang, H. Dong, J. Jie, X. Xu, J. Liu, L. He, L. Xu, W. Hu, X. Zhang, *Mater. Today* **2019**, *24*, 17.
- [141] Y. Mishima, M. Akiyama, K. Hashimoto, N. Watanabe, T. Kamata, *SID Symp. Dig. Tech. Pap.* **2017**, *48*, 176.
- [142] X. Zhang, W. Deng, B. Lu, X. Fang, X. Zhang, J. Jie, *Nanoscale Horiz.* **2020**, *5*, 1096.
- [143] D. Karnaushenko, D. Makarov, C. Yan, R. Streubel, O. G. Schmidt, *Adv. Mater.* **2012**, *24*, 4518.
- [144] D. Karnaushenko, D. Makarov, M. Stöber, D. D. Karnaushenko, S. Baunack, O. G. Schmidt, *Adv. Mater.* **2015**, *27*, 880.
- [145] A. C. Arias, S. E. Ready, R. Lujan, W. S. Wong, K. E. Paul, A. Salleo, M. L. Chabinyc, R. Apte, R. A. Street, Y. Wu, P. Liu, B. Ong, *Appl. Phys. Lett.* **2004**, *85*, 3304.
- [146] J. Tsutsumi, S. Matsuoka, T. Kamata, T. Hasegawa, *Org. Electron.* **2018**, *55*, 187.
- [147] B. Peng, J. Lin, P. K. L. Chan, in *Proc. SPIE*, **2013**.
- [148] J. Sun, A. Sapkota, H. Park, P. Wesley, Y. Jung, B. B. Maskey, Y. Kim, Y. Majima, J. Ding, J. Ouyang, C. Guo, J. Lefebvre, Z. Li, P. R. L. Malenfant, A. Javey, G. Cho, *Adv. Electron. Mater.* **2020**, *6*, 1901431.
- [149] J. Park, S. Shrestha, S. Parajuli, Y. Jung, G. Cho, *Flex. Print. Electron.* **2021**, *6*, 44005.
- [150] M. Kuang, L. Wang, Y. Song, *Adv. Mater.* **2014**, *26*, 6950.
- [151] B. Bao, J. Jiang, F. Li, P. Zhang, S. Chen, Q. Yang, S. Wang, B. Su, L. Jiang, Y. Song, *Adv. Funct. Mater.* **2015**, *25*, 3286.
- [152] C. Zhao, H. Li, Y. Wang, K. Li, J. Hou, Y. Ma, M. Li, Y. Song, *Adv. Opt. Mater.* **2019**, *7*, 1900127.
- [153] M. Kuang, J. Wang, B. Bao, F. Li, L. Wang, L. Jiang, Y. Song, *Adv. Opt. Mater.* **2014**, *2*, 34.
- [154] B. Bao, M. Li, Y. Li, J. Jiang, Z. Gu, X. Zhang, L. Jiang, Y. Song, *Small* **2015**, *11*, 1649.
- [155] K. Li, T. Li, T. Zhang, H. Li, A. Li, Z. Li, X. Lai, X. Hou, Y. Wang, L. Shi, M. Li, Y. Song, *Sci. Adv.* **2021**, *7*, eabh1992.
- [156] J. Jiang, B. Bao, M. Li, J. Sun, C. Zhang, Y. Li, F. Li, X. Yao, Y. Song, *Adv. Mater.* **2016**, *28*, 1420.
- [157] W. Deng, X. Zhang, L. Wang, J. Wang, Q. Shang, X. Zhang, L. Huang, J. Jie, *Adv. Mater.* **2015**, *27*, 7305.
- [158] X. Zhang, W. Deng, R. Jia, X. Zhang, J. Jie, *Small* **2019**, *15*, 1900332.
- [159] W. Deng, J. Jie, X. Xu, Y. Xiao, B. Lu, X. Zhang, X. Zhang, *Adv. Mater.* **2020**, *32*, 1908340.
- [160] H. Akkerman, B. Peeters, A. van Breemen, S. Shanmugam, D. Tordera, J.-L. van der Steen, A. J. Kronemeijer, P. Malinowski, F. De Rooze, D. Cheyns, J. Genoe, W. Dehaene, P. Heremans, G. Gelinck, *SID Symp. Dig. Tech. Pap.* **2018**, *49*, 494.
- [161] J.-L. P. J. van der Steen, L. C. J. M. Peters, E. C. P. Smits, P. Zalar, G. H. Gelinck, in *2019 IEEE Int. Conf. on Flexible and Printable Sensors and Systems*, IEEE, Piscataway, NJ **2019**, pp. 1–3.
- [162] H. Gold, A. Petritz, E. Karner-Petritz, A. Tschopp, J. Groten, C. Prietl, G. Scheipl, M. Zirkel, B. Stadlober, *Phys. Status Solidi* **2019**, *13*, 1900277.
- [163] M. L. Hammock, A. Chortos, B. C.-K. Tee, J. B.-H. Tok, Z. Bao, *Adv. Mater.* **2013**, *25*, 5997.
- [164] M. Han, L. Chen, K. Aras, C. Liang, X. Chen, H. Zhao, K. Li, N. R. Faye, B. Sun, J.-H. Kim, W. Bai, Q. Yang, Y. Ma, W. Lu, E. Song, J. M. Baek, Y. Lee, C. Liu, J. B. Model, G. Yang, R. Ghaffari, Y. Huang, I. R. Efimov, J. A. Rogers, *Nat. Biomed. Eng.* **2020**, *4*, 997.
- [165] S. Y. Hong, Y. H. Lee, H. Park, S. W. Jin, Y. R. Jeong, J. Yun, I. You, G. Zi, J. S. Ha, *Adv. Mater.* **2016**, *28*, 930.
- [166] C. Xie, F. Yan, *Small* **2017**, *13*, 1701822.
- [167] Q. Pan, S. Chen, M. Su, P. Li, Z. Zhang, X. Hu, G. Chen, Z. Huang, B. Chen, S. Chen, Y. Song, *Adv. Opt. Mater.* **2020**, *8*, 2000370.
- [168] Z. Gu, Y. Wang, S. Wang, T. Zhang, R. Zhao, X. Hu, Z. Huang, M. Su, Q. Xu, L. Li, Y. Zhang, Y. Song, *Nano Res.* **2021**, <https://doi.org/10.1007/s12274-021-3700-9>.
- [169] R. Jansen-van Vuuren, A. Armin, A. K. Pandey, P. L. Burn, P. Meredith, *Adv. Mater.* **2016**, *28*, 4766.
- [170] R. A. Lujan, R. A. Street, *IEEE Electron Device Lett.* **2012**, *33*, 688.
- [171] T. Zou, C. Chen, B. Xiang, Y. Wang, C. Liu, S. Zhang, H. Zhou, in *2019 Int. Electron Devices Meeting*, **2019**, pp. 8.5.1–8.5.4.
- [172] M. Melzer, M. Kaltenbrunner, D. Makarov, D. Karnaushenko, D. Karnaushenko, T. Sekitani, T. Someya, O. G. Schmidt, *Nat. Commun.* **2015**, *6*, 6080.
- [173] D. Makarov, M. Melzer, D. Karnaushenko, O. G. Schmidt, *Appl. Phys. Rev.* **2016**, *3*, 11101.
- [174] W. B. Han, G.-J. Ko, T.-M. Jang, S.-W. Hwang, *ACS Appl. Electron. Mater.* **2021**, *3*, 485.
- [175] J. Zhao, Z. Wei, Z. Li, J. Yu, J. Tang, G. Zhang, Z. Wang, *Adv. Funct. Mater.* **2021**, *31*, 2105480.
- [176] J. C. Yang, J. Mun, S. Y. Kwon, S. Park, Z. Bao, S. Park, *Adv. Mater.* **2019**, *31*, 1904765.
- [177] X. Xue, T. Zhao, X. Tian, L. Yuan, Z. Wang, T. Li, J. Zhang, *Adv. Mater. Technol.* **2021**, *n/a*, 2100849.
- [178] W. Gao, H. Ota, D. Kiriya, K. Takei, A. Javey, *Acc. Chem. Res.* **2019**, *52*, 523.
- [179] Y. Yu, H. Y. Y. Nyein, W. Gao, A. Javey, *Adv. Mater.* **2020**, *32*, 1902083.
- [180] W. Gao, S. Emaminejad, H. Y. Y. Nyein, S. Challa, K. Chen, A. Peck, H. M. Fahad, H. Ota, H. Shiraki, D. Kiriya, D.-H. Lien, G. A. Brooks, R. W. Davis, A. Javey, *Nature* **2016**, *529*, 509.
- [181] N. Tang, Y. Zheng, X. Jiang, C. Zhou, H. Jin, K. Jin, W. Wu, H. Haick, *Micromachines* **2021**, *12*, 430.
- [182] G. H. Gelinck, H. E. A. Huitema, E. van Veenendaal, E. Cantatore, L. Schrijnemakers, J. B. P. H. van der Putten, T. C. T. Geuns,

- M. Beenhakkers, J. B. Giesbers, B.-H. Huisman, E. J. Meijer, E. M. Benito, F. J. Touwslager, A. W. Marsman, B. J. E. van Rens, D. M. de Leeuw, *Nat. Mater.* **2004**, 3, 106.
- [183] P. Andersson Ersman, R. Lassnig, J. Strandberg, D. Tu, V. Keshmiri, R. Forchheimer, S. Fabiano, G. Gustafsson, M. Berggren, *Nat. Commun.* **2019**, 10, 5053.
- [184] R. Kwok, *Nature* **2013**, 497, 176.
- [185] E. P. Gardner, J. H. Martin, T. M. Jessell, in *Principles of Neural Science* (Eds: E. Kandel, J. Schwartz, T. Jessell). McGraw-Hill. New York, NY, USA, **2000**.
- [186] Y. Kato, T. Sekitani, Y. Noguchi, M. Takamiya, T. Sakurai, T. Someya, in *IEEE Int. Electron Devices Meeting*, IEEE, Piscataway, NJ **2008**, pp. 1–4.
- [187] J. Liu, X. Zhang, Y. Liu, M. Rodrigo, P. D. Loftus, J. Aparicio-Valenzuela, J. Zheng, T. Pong, K. J. Cyr, M. Babakhanian, J. Hasi, J. Li, Y. Jiang, C. J. Kenney, P. J. Wang, A. M. Lee, Z. Bao, *Proc. Natl. Acad. Sci. U. S. A.* **2020**, 117, 14769.
- [188] Y. Kato, T. Sekitani, Y. Noguchi, M. Takamiya, T. Sakurai, T. Someya, T. Yokota, M. Takamiya, T. Sakurai, T. Someya, *IEEE Trans. Electron Devices* **2010**, 57, 995.
- [189] M. Zirkl, A. Sawatdee, U. Helbig, M. Krause, G. Scheipl, E. Kraker, P. A. Ersman, D. Nilsson, D. Platt, P. Bodö, S. Bauer, G. Domann, B. Stadlober, *Adv. Mater.* **2011**, 23, 2069.
- [190] Y. Qin, H. Wang, Y. Liu, *SID Symp. Dig. Tech. Pap.* **2018**, 49, 1604.
- [191] Z. Zhang, L. Chen, X. Yang, T. Li, X. Chen, X. Li, T. Zhao, J. Zhang, *IEEE Electron Device Lett.* **2019**, 40, 111.



Bin Bao is currently a postdoctoral researcher at the Leibniz Institute for Solid State and Materials Research Dresden (Leibniz IFW Dresden), Germany. He received his Ph.D. degree in physical chemistry from Institute of Chemistry, Chinese Academy of Sciences in 2015 under the supervision of Prof. Yanlin Song. His research focuses on flexible and printable electronic devices.



Dmitriy D. Karnaushenko received the Dr.-Ing. degree from Chemnitz University of Technology, Chemnitz, Germany, in 2017, for his work on self-assembled helical antennas. He started as a postdoctorate researcher at the Leibniz Institute for Solid State and Materials Research Dresden (Leibniz IFW Dresden), Germany, in 2017. His research focuses on self-assembling electronic devices, FEM simulations for mechanical, and electrical and microfluidic devices.



Oliver G. Schmidt received the Dr.rer.nat. degree from TU Berlin, Berlin, Germany, in 1999. From 2007 to 2021, he was the director of the Institute for Integrative Nanosciences, Leibniz IFW Dresden, Germany. He holds a full professorship for materials systems for nanoelectronics at Chemnitz University of Technology, Chemnitz, Germany. He is an adjunct professor for nanophysics at Dresden University of Technology, and holds an honorary professorship at Fudan University, Shanghai, China. His interdisciplinary activities bridge across several research fields, ranging from flexible electronics and microrobotics to energy storage and nanophotonics.



Yanlin Song received his Ph.D. degree from the Department of Chemistry at Peking University in 1996. He then worked as a postdoctoral fellow in the Department of Chemistry of Tsinghua University from 1996 to 1998. He joined the Institute of Chemistry, Chinese Academy of Sciences, in 1998. He is currently a professor and director of Key Laboratory of Green Printing, Chinese Academy of Sciences. His research interests include information function materials, photonic crystals, printed electronics, and green printing materials and technologies.



Daniil Karnaushenko received the Dr.-Ing. degree from Chemnitz University of Technology, Chemnitz, Germany, in 2016, for his work on shapeable electronics, after studying at Novosibirsk State Technical University, Novosibirsk, Russia. He started as a postdoctorate researcher at the Leibniz Institute for Solid State and Materials Research Dresden (Leibniz IFW Dresden), Dresden, Germany, in 2016. Currently, he is a group leader at the research center MAIN at Chemnitz University of Technology. His research focuses on novel microfabrication processes, including self-assembly techniques and microelectronics.